HHS Public Access

Author manuscript

Environ Monit Assess. Author manuscript; available in PMC 2022 June 24.

Published in final edited form as:

Environ Monit Assess. ; 193(7): 440. doi:10.1007/s10661-021-09213-9.

Investigation of Pb-contaminated soil and road dust in a polluted area of Philadelphia

Michael J. O'Shea[1,*], **Mark P.S. Krekeler**[2,3], **David R. Vann**[1], **Reto Gieré**[1,4]

[1]Department of Earth and Environmental Science, University of Pennsylvania, Philadelphia, PA 19104-6316, USA

[2]Department of Geology and Environmental Earth Science, Miami University Hamilton, Hamilton, OH 45011, USA

[3]Department of Geology and Environmental Earth Science, Miami University, Oxford, OH 45056, USA

[4]Center of Excellence in Environmental Toxicology, University of Pennsylvania, Philadelphia, PA 19104-6316, USA

Abstract

A multi-analytical geochemical investigation of Pb-contaminated collocated road dust and soils, at two size fractions, was performed in Fishtown, Philadelphia, PA, USA. The combinations of methods employed in this case study were chosen to better characterize the contamination, enhance identification of pollution sources, improve understanding of the impact of former Pb smelters, and to study the relationships between two media and between two size fractions. High concentrations of Cu and Sn were observed in both bulk and finer road dust, whereas large concentrations of Zn and Pb were found in both bulk and finer soil samples, implying pollution. There were no obvious associations between Pb soil concentrations and former smelter locations. Therefore, the primary source of the high mean Pb content in bulk (595 ppm) and fine soils (687 ppm) was likely legacy lead paint and/or leaded-gasoline products. Using electron microscopy, we found that Pb particles were mainly 0.1–10 μm in diameter and were ubiquitous in both soil and dust samples. Two-way analysis of variance tests revealed that, for most chemical elements explored here, there were statistically significant differences in concentrations based on media and size fractions, with finer sizes being more polluted than bulk. The mineralogical composition and the sources of several pollutant elements (Cr, Cu, Zn, Pb), however, were similar for both soil and dust, pointing to material exchange between the two media. We suggest that future investigations of collocated road dust and soils in urban environments use the methodologies applied in this study to obtain detailed insights into sources of roadside pollution and the relationships between neighboring media.

[*]Corresponding author: michajo@sas.upenn.edu.

Authors' contributions: CRediT authorship statement: MJO: Conceptualization, Methodology, Investigation, Writing - original draft, Writing - review & editing, Visualization. MPSK: Methodology, Investigation, Writing - review & editing, Visualization. DRV: Methodology, Writing - review & editing, Visualization. RG: Conceptualization, Writing - review & editing, Supervision, Funding acquisition.

Conflicts of interest/competing interests: The authors declare that they have no conflicts of interest to declare that are relevant to the content of this article.

Keywords

Lead (Pb); pollution; multi-media; multi-analytical; roadside hazards; electron microscopy

Introduction

Contamination of urban environments is of mounting concern due to growing populations and increased urbanization (United Nations, 2014). The consequences of intensifying soil and air pollution as a byproduct of expanding cities and peri-urban spaces need to be fully explored (Alves et al., 2020; Kong et al., 2011; Lim et al., 2012). This pollution represents a potential human health hazard (e.g., Adimalla, 2020; Alves et al., 2020; Ferreira-Baptista and De Miguel, 2005). Environmental media, such as urban road dust and soils, can be used to better assess the impacts on health caused by the pollution (e.g., Acosta et al., 2015; Christofordidis and Stamatis, 2009; Ordonez et al., 2003; Padoan et al., 2017).

Urban road dust is defined as particles that collect on impervious outdoor surfaces, such as roadways or parking lots (e.g., Liu et al., 2014). These particles consist of a wide array of materials of anthropogenic or natural origin (Pant and Harrison, 2013; Shi et al., 2011; Teran et al., 2020; Thorpe and Harrison, 2008) and include dust from local soils, industrial activities, and both exhaust and non-exhaust traffic emissions (Pant and Harrison, 2013; Thorpe and Harrison, 2008; Varrica et al., 2003). Road dust and soil particles that are small enough can be re-suspended by vehicles' movement and wind, potentially contributing to particulate air pollution (Amato et al., 2009; Laidlaw et al., 2012). As a result of its interactions with local soil and atmosphere, road dust is both source and sink for pollutants (Biasioli et al., 2006; Christoforidis and Stamatis, 2009). Consequently, soils and road dust have been studied to determine contamination in the urban environment (e.g., Bavec et al., 2014; Dietrich et al., 2019; Filippelli et al., 2015; Filippelli et al., 2020; Gaberšek and Gosar, 2018; Gaberšek et al., 2020; Gaberšek and Gosar, 2021; Laidlaw and Filippelli, 2008; Laidlaw et al., 2017; Padoan et al., 2017).

Previous assessments of road dust and soils were typically focused on bulk elemental concentrations (e.g., Apeagyei et al., 2011; Lanzerstorfer, 2020; Wei and Yang, 2010) and less frequently included descriptions of mineralogical composition or particle size distributions, organic content, and/or particle morphology (e.g., Dietrich et al., 2018; Gaberšek and Gosar, 2021; Gunawardana et al., 2012; Legalley and Krekeler, 2013; O'Shea et al., 2020; Padoan et al., 2017). Some previous inquiries examined both road dust and soils, (e.g., Acosta et al., 2015; Kelepertzis et al., 2020; Kelepertzis et al., 2021; Ordonez et al., 2003) but few performed collocated sampling (e.g., Christofordidis and Stamatis, 2009; Padoan et al., 2017).

Humans are primarily exposed to pollutants in road dust and soils through ingestion, inhalation, and epidermal contact (Ferreira-Baptista and De Miguel, 2005). For most road-dust and soil particles, ingestion is the primary exposure pathway (Ruby and Lowney, 2012; Siciliano et al., 2009). The dangers of contaminated soil or road-dust ingestion have been documented by previous investigations (e.g., Agency for Toxic Substances and Disease

Registry (ATSDR), 2019; Calabrese et al., 1997; Davis and Mirick, 2006; Elom et al., 2014; Okorie et al., 2012; Stanek et al., 1997; Stanek et al., 2012).

Philadelphia, PA, was chosen as the field location for the current study. The climate in Philadelphia is typical for the Northeastern United States, having a mean annual temperature of 12.25 °C, an average annual precipitation >100 cm, with a dominant SW wind (NOAA, 2019). These factors and the local geological formations, traffic activity, land use, industrial activity, commercial activity, and roadway materials were inferred to have influenced the composition and transport of road dust and soils (e.g., O'Shea et al., 2020). A prominent local geological unit, exposed in numerous places across the city, is the Wissahickon Formation, consisting largely of Wissahickon schist of which the principal minerals are quartz, mica, and plagioclase (Weiss, 1949).

Philadelphia, founded in 1682, is known for its long history of shipping and industry. Former sources of industrial pollution (e.g., Cr, Hg, Pb) in Philadelphia include chemical processing, tanning, metalworking, and textile production (e.g., Scranton, 1989). In addition, Pb smelting was a major industry, primarily from the late 19th century through the mid 20th century. At one point, Philadelphia had 36 active Pb smelters (Lusby et al., 2015; Ruderman et al., 2017a), and thus, Pb pollution is a major concern. Exposure to Pb has well-documented human health impacts: it can result in the development of neurobehavioral disorders and reduced cognitive abilities, with toxicity affecting most internal organs (Council on Environmental Health, 2016; Lanphear et al., 2005; Latimer et al., 2016; Tong et al., 2000). Children are at the highest risk for ingesting Pb-contaminated soils and road dust due to their high rates of hand-to-mouth contact compared with adults and for physiological reasons (e.g., Council on Environmental Health, 2016; Ko et al., 2007; United States Environmental Protection Agency [USEPA], 2001).

The River Wards in Northeastern Philadelphia, including our study area, Fishtown, are home to many former Pb smelters. A previous study in Philadelphia found that concentrations of Pb in soils were higher near former Pb smelters compared with residential sites (Lusby et al., 2015). However, the authors also noted that Pb contamination is likely widespread and not limited to areas near former smelters (Lusby et al., 2015). Other primary sources of Pb include legacy Pb paint, which has been identified as a major source of Pb poisoning across the globe (e.g., (e.g., Gieré et al., 2020; Laidlaw and Taylor, 2011; Lusby et al., 2015; O'Shea et al., 2021; Turner et al., 2016; Turner and Sogo, 2012; Turner and Solman, 2016). A study of national blood Pb level (BLL) data in the U.S. noted that dust in and near homes from Pb paint was a good predictor of BLLs in children (Lanphear et al., 1998). Furthermore, an investigation using French data found that most children with elevated BLLs resided in homes with Pb paint (Pichery et al., 2011). Another key source of Pb pollution is leaded-gasoline (e.g., Filippelli et al., 2020; Lusby et al., 2015; Shotyk et al., 2002; Weiss et al., 1999). Previous research found that the ban of leaded gasoline led to a dramatic decrease of Pb concentrations in road dust ten years following its prohibition (MacKinnon et al., 2011). However, this was not the case for soils or vegetation, demonstrating that Pb is persistent in the environment (MacKinnon et al., 2011). Additionally, resuspension of soil and dust is often associated with seasonally elevated BLLs (e.g., Filippelli et al., 2005; Laidlaw and Filippelli, 2008; Laidlaw et al., 2012; Filippelli

et al., 2020). Indeed, Pb concentrations in soils and children's BLLs are intimately linked (Mielke et al., 2019).

The primary goal of the present study was to examine the level of pollution in road dust and soils at collocated sites. We investigated two different size fractions of these media to assess elemental distributions and to specifically better understand the distribution of Pb near historic sources. We used a multi-analytical approach that provides a framework for future investigations to better assess pollution sources and relationships between collocated media.

Methods

Road-dust and soil samples were collected in October 2017. All sampling took place before the first snowfall to avoid the presence of winterizing agents.

Road-dust sampling

Twenty sites within the Fishtown neighborhood of Philadelphia were selected for sampling (Figure 1). Some sites were chosen because of their proximity to former smelting locations. The remaining sites were semi-randomly selected in a grid pattern, provided that they were adjacent to publicly accessible soil patches. We focused on streets in residential areas; highways were not sampled. Road dust was collected according to the methods described in O'Shea et al. (2020).

Soil sampling

Collocated soil samples were obtained within 2 m of the sites where road dust was collected. Public spaces were targeted for this assessment due to the ease of access and their proximity to the streets. At each site, five random subsamples within one square meter were removed from the top 5 cm of soil using disposable plastic spoons (e.g., Acosta et al., 2015; Padoan et al., 2017). The five subsamples were combined into a single sample, which was then homogenized in a polyethylene bag by vigorous shaking for five minutes (e.g., Padoan et al., 2017; Wei et al., 2010). A new spoon was used at each site.

Analytical methods

All road-dust and soil samples were dried in an oven at 100°C for five hours prior to analysis (Faiz et al., 2009; Wei et al., 2014). After drying, each dust and soil sample was dry sieved using an 841-μm (No. 20 mesh) stainless-steel hand-held sieve (O'Shea, et al., 2020). Below, the size fraction passing through this sieve is referred to as bulk dust (BD) or bulk soil (BS). The sample weights for BD ranged from 23–222 g, whereas the BS weight range was 32–156 g. Sufficient BD and BS were set aside for subsequent analysis by X-ray powder diffraction (XRD), inductively coupled plasma-optical emission spectrometry (ICP-OES), scanning electron microscopy (SEM), transmission electron microscopy (TEM), and for the determination of loss on ignition (LOI). The remaining portion of each sample was sieved to <125 μm utilizing a stainless-steel hand-held sieve (No. 120 mesh) to produce a more health-relevant size fraction. This finer fraction is referred to as fine dust (FD) or fine soil

(FS). Note that, as a result of the sample-preparation procedure, BD and BS also contain the size fraction <125 μm.

In this study, laser diffraction was only performed on ashed FD and FS samples. Ashing was executed to remove organic matter that could interfere with particle size results. For ashing and determination of LOI, samples (2 g) were weighed using a Sartorius analytical balance before and after being placed in a muffle furnace (Thermolyne model 6000) at 500 °C for 8 h, following the protocol outlined in O'Shea et al. (2020). All other analyses were completed on the non-ashed samples.

Methods and standards used for analysis were those described in O'Shea et al. (2020). Briefly, XRD was performed using a Panalytical X'Pert Powder X-ray Diffractometer equipped with a Co-Kα radiation source set to 40 kV and 40 mA. Weight percentages of each mineral phase were estimated with the reference intensity-ratio technique. For the determination of LOI, two g of each sample were weighed before and after muffling (Thermolyne model 6000 furnace) at 500°C for eight hours (Ball, 1964). Laser diffraction of the ashed FD and FS was performed using a Beckman-Coulter LS 13 320 Particle Size Analyzer. A hydrochloric/nitric acid digest (comparable to Method-3050B; USEPA, 1996), designed to test environmental availability, was used to prepare samples for analysis by ICP-OES (Genesis, Spectro GMBH). The elements analyzed were Na, Mg, Al, P, K, Ca, Ti, V, Cr, Mn, Fe, Co, Ni, Cu, Zn, Cd, Sn, Sb, Hg, and Pb. These elements were chosen as they are commonly expected from local geological and pollution sources (see O'Shea et al., 2020). All analytical data as well as other relevant information on land use, road surface, and traffic are provided for each site in the supplemental file (Table S1a, b).

SEM was used to investigate selected road-dust ($n = 4$) and soil ($n = 4$) samples. Characterization was performed with a Zeiss Supra 35 VP electron microscope equipped with a field-emission gun (FEG), an Energy-Dispersive X-ray (EDX) spectrometer, and a backscatter electron detector. Samples were mounted on 12.7 mm SEM aluminum stubs with conductive carbon tabs. The instrument was used in backscatter electron (BSE) and variable-pressure modes for imaging. Nitrogen (N_2) was used as the compensating gas for variable-pressure mode as in Dietrich et al. (2018). This approach is very similar to that used in previous investigations of road dust (e.g., LeGalley and Krekeler [2013], Flett et al. [2016], and Dietrich et al. [2019]).

TEM was performed on the two soil samples containing the highest Pb and Zn concentrations, respectively (FS at sites 1 and 19). Only soil samples were analyzed due to instrument time constraints and because of the complexity and detail required of the data collection. Furthermore, soil samples were most polluted with Pb (see "Results and Discussion" section), and soil is known to be a medium capable of storing traces of pollution through time (e.g., Qiao et al., 2014). To prepare the samples for TEM, a small amount of soil was suspended in approximately 2 mL of ethanol in a small glass container and vigorously shaken. Then, two aliquots of approximately 20 μL were placed sequentially onto a 3-mm copper grid with lacey-carbon film and allowed to air dry between additions. A JEOL JEM-2100 transmission electron microscope with a Bruker EDX detector was used for bright-field imaging and chemical analysis. The instrument was operated at 200 kV.

Images were taken with a Gatan Orius SC 200D CCD camera. High-resolution images and selected-area electron diffraction (SAED) patterns were used to determine crystallinity, whereas EDX mapping was used for element identification. Similar approaches have been used in a previous investigation of road dust (LeGalley and Krekeler, 2013) as well as in other studies of fine-grained materials (Barnes et al., 2020; Cymes et al., 2020, Paul et al., 2017).

EDX analysis of fine-grained mixed media samples with multiple components is challenging, and careful attention must be given to peak overlap and the limitations of signal contributions from multiple minerals or phases. Lines used to identify elements provided by Bruker software include O-K = 0.525 keV; Na-K 1.040 keV; Mg-K = 1.254 keV; Al-K= 1.487 keV; Si-K_α = 1.740 keV (nominally K_β = 1.837 keV); P-K_α = 2.010 keV (nominally K_β = 2.139 keV); S-K_α = 2.309 keV (nominally K_β = 2.465 keV); Cl-K_α = 2.621 keV (nominally K_β = 2.812 keV); K-K_α = 3.312 keV and K-K_β = 3.590 keV; Ca-K_α = 3.691 keV and Ca-K_β = 4.013 keV; Ti-K_α = 4.509 keV and Ti-K_β = 4.934 keV; Cr-K_α = 5.410 keV and Cr-K_β = 5.947 keV; Mn-K_α = 5.895 keV and Mn-K_β = 6.492 keV; Fe-K_α = 6.399 keV and Fe-K_β = 7.060 keV; Cu-K_α = 8.036 keV and Cu-K_β = 8.903 keV; Zn-K_α = 8.626 keV and Zn-K_β = 9.570 keV; Pb-L_α = 10.541 keV (nominally M $_\alpha$ = 2.342 keV, M_β = 2.444 keV). Common lines that overlap are Mn-K_β = 6.492 keV and Fe-K_α = 6.399 keV when present, and potentially S-K_α = 2.309 keV (nominally K_β = 2.465 keV) and Pb-M $_\alpha$ = 2.342 keV and Pb-M_β = 2.444 keV. Lead is identified only when a Pb-L_α line is evident, and Mn was identified based on the Mn-K_α line. Although both S and Pb may be present in spectra containing Pb lines, Pb-L_α, -M $_\alpha$, and -M_β lines are in the correct position, proportion, and intensity for Pb only for both SEM and TEM data. If S was present in Pb spectra, it was interpreted to occur in minor amounts. Moreover, SAED patterns never pointed to the presence of a S-bearing Pb phase (e.g., PbS or $PbSO_4$). Carbon sticky tabs, the ubiquitous nature of O, and Al stubs may contribute to some of the EDX spectra for SEM data. The ubiquitous nature of O and scatter from the Cu grid and the lacey-C substrates contribute to TEM-EDX spectra.

The rationale for using the above combination of methods was to investigate comprehensively the mineralogical (XRD), chemical (ICP-OES, EDX), and physical (laser diffraction, loss on ignition, SEM and TEM analysis) properties of two collocated environmental media in unprecedented detail. Furthermore, electron microscopy is rarely used in this area of pollution research, even though it allows for sample characterization at multiple scales, providing invaluable insight into particle morphology, composition, and crystallinity. The main advantage of our expanded, holistic approach is that it facilitates a uniquely detailed materials characterization, which aids in the interpretation of the sources of environmental pollution. In addition, it enables exploring the interactions between dust and soil in two size fractions. Because many past studies focused on only one medium and one size fraction and used few analytical techniques, our work represents one of the most comprehensive roadside pollution assessments performed to date. The approaches utilized here may be applied in similar locations to determine the nature and potential risk of contamination.

Statistical analysis

Statistical tests performed on the elemental concentrations followed O'Shea et al. (2020), which included descriptive statistics, Spearman's correlations coefficients (called Spearman correlations herein), and varimax rotated factor analysis separated by major and minor elements. The major element group included Na, Mg, Al, P, K, Ca, Ti, and Fe, whereas V, Cr, Mn, Co, Ni, Cu, Zn, Cd, Sn, Sb, Hg, and Pb were assigned to the minor element category. The normality of the elemental concentrations in all fractions was determined using a Shapiro-Wilk test, and most elementals had non-normal distributions. Therefore, factor analysis was performed on the Spearman-ranked correlation matrices of the elemental concentrations. Additionally, two-way analysis of variance (ANOVA) tests of the log-normalized data were performed for each element to determine the statistical significance ($p<0.05$) of size fraction and media for the concentrations found. Interaction terms were also determined for all elements in the ANOVA tests. As significant results were found in many cases, we proceeded with post-hoc tests (Tukey's honestly significant difference [HSD]). Finally, mean elemental concentrations were normalized to the respective mean concentrations in both the continental crust (Rudnick & Gao, 2003) and the local Wissahickon Formation (e.g., O'Shea et al., 2020).

Results and discussion

Particle size, LOI, and mineral phases

Figure 2 displays both average (FD, n=20; FS, n=20) and cumulative particle volumes, obtained by laser diffraction. The shape of the average volume curves for FD and FS were quite different; the FD curve steadily increased with increasing particle size, whereas the values for FS increased continuously until approximately 70 μm, where it plateaued before it started to decrease from about 100 μm. Notably, the mean particle size was higher for the FD (99 μm) than for the FS (73 μm) samples. Using the graphic results, particles less than 10 μm in diameter, PM_{10}, comprised 4% of the total FD volume, compared with 6% for FS.

The LOI values of BS and FS were virtually indistinguishable (Figure 3). Similarly, the LOI values of BD and FD were nearly identical. However, the mean LOI values of both BS (10.8 wt%) and FS (11.2 wt%) were considerably higher than those of BD (6.6 wt%) and FD (7.0 wt%), which was expected, as the LOI data probably reflect mostly organic content.

The main mineral phases identified in all media and fractions were quartz, dolomite, calcite, and plagioclase (Table 1). The estimated mineral abundances show that road dust (BD and FD) was typically poorer in quartz but richer in dolomite/calcite and feldspar compared with soils (BS and FS). Therefore, some of the road dust appears be derived from the road aggregate, sidewalk (concrete), and/or concrete construction materials, all of which often contain calcite and dolomite (see also Gillott, 1978; El. Machi et al., 2021; O'Shea et al., 2020; Sommer et al., 2018). In contrast, mica and/or chlorite were found in BS, FS, and BD but not in FD, suggesting that runoff water and/or wind systematically removed fine mica flakes from the roadways, even if soils are regularly contributing to road-dust composition. Other phases identified by XRD included rutile and possibly halloysite. Despite the differences observed, many of the identified phases occurred in both road dust

(BD and FD) and soil (BS and FS), indicating potential interaction between media. Some of the quartz, feldspar, mica, and rutile detected in road dust could be derived from the Wissahickon Formation, as described in O'Shea et al. (2020).

Major elements

Data from the elemental analyses are summarized in Figure 4 (see also Table S2a,b). Among the major elements, Mg and Ca were present at statistically significantly higher concentrations in the road dust (BD and FD) than in soil (BS and FS) (Table 2). The correlation between the Mg and Ca concentrations was statistically highly significant in all sample types ($R \geq 0.93$ $p < 0.05$) (Table S3a,b). These correlations were consistent with the presence of dolomite in the roadway and neighboring soils. Overall, there were more statistically significant ($p < 0.05$) Spearman correlations in the finer fraction (14 for FD, 13 for FS) than in the bulk (seven BD, five for BS). Compared to the continental crust (CC), all major elements were depleted, except for P (for all media and fractions) and Ca (for only FD), which showed normalized values >1.0 (Table S4). Relative to the local Wissahickon Formation (WF), P and Ca were strongly enriched (>1.0) in all fractions and media (Table S4). In addition, Fe was also enriched relative to the WF in all sample types, potentially reflecting inputs from traffic (e.g., Apeagyei et al., 2011; Herngren et al., 2006). Magnesium was enriched relative to the WF in BD, FD, and FS. However, Na, Al, K, and Ti were depleted relative to the WF for all fractions and media. The depletions of two of these elements, Al and K, could partially be due to the absence of mica in 12 of the 20 sample sites (Table 1). It should be pointed out that, as we used an environmentally focused acid extraction technique, lower elemental concentrations would be expected in our samples than in the cases of WF and CC, which represent whole-rock analyses preceded by total digestion. Therefore, the observed enrichments in Mg, P, Ca, and Fe relative to the WF would most likely be even more pronounced, if we would have performed a total digestion. For most major elements (Mg, Al, P, Ca, Ti, and Fe), acid-leachable concentrations were higher in the finer size fraction of both soil and dust than in the respective bulk samples (Figure 4). Previous investigations also observed that finer size fractions generally contained higher concentrations of elements compared with larger fractions (e.g., Kong et al., 2011; Lanzerstorfer, 2018; Padoan et al., 2017; Zannoni et al., 2016; Zhao et al., 2010). Some elements were more concentrated in FD (Mg, Ca, Ti, Fe) than in FS, whereas others were more abundant in FS (Na, Al, P, K) than in FD (Figure 4). To find out whether or not the differences observed between major element concentrations for both size and media were statistically significant ($p < 0.05$), two-way ANOVA tests were performed. These tests revealed that, for all soil samples (BS+FS) compared with all dust samples (BD+FD), there were statistically significant differences for Mg, Al, P, Ca, Ti, and Fe concentrations (Table 2). There were also statistically significant differences between all bulk samples (BS+BD) and all finer samples (FS+FD) for Na, Mg, Al, P, K, Ca, and Ti concentrations (Table 2).

Factor analysis for the major elements revealed that three factors explained the majority of the cumulative variance in BD, FD, and FS (Table 3, S5a, S5b). However, for BS, four factors were necessary to explain the variance. Factor 1 for all media and fractions was always driven by Mg and Ca, again highlighting dolomite derived from road aggregate, sidewalk materials, and/or construction materials as a source. Factors 2 and 3, for all media

and fractions, were driven by a similar group of elements (mainly, K, Al, Fe, Na, Ti, and P), which most likely reflect the importance of the WF (e.g., micas, albite, rutile) as source (e.g., Weiss, 1949). However, P is not abundant in the WF and all samples were enriched (≥1.89x) in P relative to this formation. Both BS (6.92x) and FS (8.81x) were considerably more enriched in P than BD (1.89x) and FD (3.15x) were; the enrichment of P in the soil samples could be due to the addition of fertilizers (e.g., Jiao et al., 2012). The P in road dust might be derived from soil, suggesting communication between the two media. Other potential sources of P in both media include motor vehicle emissions and/or construction activity (e.g., Novotny and Chesters, 1981). Factor 4 for BS (Fe, Al, and P) could represent traffic or possibly industrial activity such as metal working; however, this was not clear. Based on the factor analysis of all types of samples, the primary sources of the major elements were interpreted as road aggregate/sidewalk/construction materials, traffic activity, and local geological formations, with fertilizer being an additional source for the soils. Overall, the similarities in presumed sources between road dust and soil imply exchange between the collocated road dust and soil.

A previous assessment of BD in Philadelphia identified three factors that explained most of the observed variance (O'Shea et al., 2020). In that report, the source of Factor 1 (dominated by K and Na) was the WF. In contrast, Factor 2 (Fe, Ca, and Ti) was primarily related to products of traffic activity, including brake-pad particles, and natural sources such as the WF. Finally, the source of Factor 3 (dominated by P and Al) was unclear. In the current investigation, P and Al were both present in Factor 2 (for both BD and BS), Factor 3 (FD), and Factor 4 (BS). Overall, many of the same sources were identified in both the past and the current Philadelphia studies, including traffic and the WF. Magnesium was not analyzed in O'Shea et al., 2020; had it been, Mg would probably have contributed strongly to a factor, along with Ca, as dolomite was identified at 28 of the 30 studied sample sites.

Minor elements

As was the case for major elements, there were more significant ($p<0.05$) Spearman correlations for the minor elements in the finer fractions (19 for FD; 14 for FS) than in the bulk samples (12 for BD; 10 for BS) (Table S6a, 6b). In all media and fractions, there were statistically significant correlations between Mn and Co (≥0.64) and between Ni and Cu (≥0.51). The correlations between Mn and Co could be associated with steel wear, whereas those between Ni and Cu could be related to traffic activities (e.g., Han et al., 2017; Zibret et al., 2013). The mean concentrations of most minor elements (V, Cr, Mn, Ni, Cu, Zn, Pb) in the finer size fraction of both soil and dust were higher than in the respective bulk samples (Figure 4). Some elements (e.g., Mn, Zn, Pb) had their highest mean concentrations in FS, whereas others (e.g., V, Cr, Ni, Cu, Sn) were more concentrated in FD (Figure 4; Table S2c, d). The higher concentrations of Cr and Cu in FD compared with FS could be related to vehicular activity (e.g., Duong and Lee, 2011; Liang et al., 2019; Zglobicki et al., 2019; Zhao et al., 2019; Zibret et al., 2013). However, the mean concentration of Zn was higher in FS than in FD, even though Zn is often associated with tire-wear particles (e.g., Harrison et al., 2012). Previous studies have demonstrated that tire-wear particles often end up in soils adjacent to roads and highways (e.g., Councell et al., 2004; Dannis, 1974; Wik and Dave, 2009). The high concentrations of Zn in FS, therefore, could suggest

communication between road dust and soil. Two-way ANOVA tests were performed to statistically examine a possible link between size/media and minor element concentrations. These tests revealed that there were statistically significant ($p<0.05$) differences between all soil samples (BS+FS) and all dust samples (BD+FD) for V, Mn, Cu, and Pb concentrations (Table 2). In terms of size, V, Cr, Mn, Co, Ni, Cu, Zn, and Sn concentrations were statistically significantly different in all finer samples (FD+FS) compared with all bulk (BD+BS) samples (Table 2). In order to assess the minor element concentrations in our samples within a more general natural framework, they were normalized to CC; copper, Zn, Sn, and Pb were highly enriched in all sample types, whereas V, Cr, Mn, Co, and Ni were depleted (Table S4). These results further highlight the contamination of the studied materials by some traffic-related elements (Cu, Zn) as well as elements associated with legacy sources (Pb from smelters, paint, and gasoline) and solder (Sn) (e.g., Lu et al., 2010; Duong and Lee, 2011; Liu et al., 2014; De Silva et al., 2016; Teran et al., 2020; Zibret et al., 2013).

Factor analysis for the minor elements revealed that four factors explained the majority of the variance in BD and BS, whereas three factors were sufficient to explain the variance in FD and FS (Table 3; Table S7a, 7b). Factor 1 for BD and Factor 1 for BS were both associated with the same elements (Co, V, Mn), which could be related to the wear of steel and other metal alloys (e.g., Han et al., 2017). Factor 1 for FD (Ni, Cr, Mn, Cu, Zn, Co) and Factor 1 for FS (Cr, Cu, Ni, Zn, Sn) probably both represent non-exhaust emissions from vehicles (e.g., Bernardino et al., 2019; Gaberšek and Gosar, 2018; Hiller et al., 2020; Teran et al., 2020; Zibret et al., 2013). Similarly, Factor 2 for BD (Cr, Sn, Zn) and Factor 3 for BS (Cr, Cu, Ni) could both be related to traffic activity. Lead has the highest factor loading in Factor 2 (≥0.87 for BS and FS) and in Factor 3 (≥0.76 for BD and FD), pointing to legacy sources of contamination in the area, i.e., smelters and Pb paint (e.g., Komarek et al., 2009; Lusby et al., 2015; Smith et al., 2011) or leaded-gasoline products (e.g., Lusby et al., 2015). Factor 2 for FD (V and Co) may be associated with alloys, but this was uncertain as discerning the varied industrial activities related to each factor was not possible. Factor 3 for FS (Co and Mn) may be linked to steel wear (e.g., Zibret et al., 2013). Factor 4 for BS (primarily Sn) could be related to solder, can coatings, and/or fossil fuel emissions (e.g., Zibret et al., 2013). The origin of Factor 4 for BD (Ni, Cu, Mn) was unclear. From the factor analysis, we posit that the primary sources of minor elements for all sizes and media were mixed industrial activity, traffic, and Pb smelters/paints/gasoline. As previously noted for major elements, similarities in sources suggest that there are likely substantial interactions between dust and soil.

Our current research is similar to a previous BD investigation in Philadelphia, which found four factors that explained most variance in minor element concentrations (O'Shea et al., 2020). In that past report, Factor 1 (Cr, Cu, Zn) was attributed to traffic, Factor 2 (V and Cr) mainly to the wear of steel and other alloys, Factor 3 (Pb) to smelters and paint, and Factor 4 (Sn) to solder, can coatings, and fossil fuel emissions. In other words, many of the same sources, including traffic, alloys, smelters, paints, solder, and emissions, were identified on the basis of the minor elements in both the past and the current study, thus providing support for the interpretations.

Mean Pb content recorded in the current investigation (209 ppm for BD) was lower than that reported in the previous analysis of bulk road dust in Philadelphia (516 ppm) (O'Shea et al., 2020). However, the median Pb concentrations in the current (147 ppm) and previous (202 ppm) BD investigations were similar, demonstrating the influence of outlier sites on the older data set.

The BD from Fishtown examined here was generally lower in minor element contents compared with values from past studies of road dust at international sites (see Table 10 in O'Shea et al., 2020). Lead concentrations in BS from Fishtown were similar to values from past investigations of soil in U.S. urban residential areas (Frank et al., 2019). However, the BS samples studied here were richer in minor elements, especially Pb and Zn, than roadside soils from a range of comparable international studies (Table 4).

The high mean Pb concentrations in our BS and FS samples were primarily driven by two sites (1 and 5; see Table S1), neither of which were within 0.25 km of former smelters (Figure 1). For FS, an additional eight sites (6, 9, 12, 13, 14, 16, 18, and 19) were above the 400 ppm threshold listed by the US EPA for bare soils where children play (Council on Environmental Health, 2016). Of these sites, six (9, 12, 13, 14, 16, and 19) were within 0.25 km of former smelters (Figure 1). However, the two sites closest to former smelters, Sites 10 and 11 (see Figure 1), had mean FS-Pb concentrations below 400 ppm (199 ppm and 117 ppm, respectively), but, to the best of our knowledge, they had not been remediated prior to our sampling campaign. On the other hand, remediation did take place in other parts of Fishtown: i) after our sampling took place, there were additional efforts (first started in 2003) to remediate Pb contamination at the former Anzon Pb-smelting complex located directly northeast of Sites 12 and 13 (see Figure 1) (e.g., Pennsylvania Department of Environmental Protection [DEP], 2021a; Ruderman et al., 2017b); ii) an area approximately 0.3 km to the northwest of Site 11 was remediated, beginning in 2006, for leaded gasoline pollution (Pennsylvania DEP, 2021b); and iii) after our sampling efforts, an area near Site 2 was remediated for leaded gasoline pollution (Pennsylvania DEP, 2021b). From our data and the information gathered on remediation efforts, we conclude that the Pb measured in soils at all our sites was largely derived from legacy Pb paint and/or leaded-gasoline products rather than from the past smelting activity.

As Pb was an important focus of this study, we examined samples microscopically to determine its physical location in the dust and soil.

Microscopy of Pb-bearing particles

The dust and soil samples richest in Pb were examined by SEM, which revealed that numerous Pb particles occur in both road dust and soils. Many of these particles are present as irregularly shaped or subrounded aggregates, which are mainly 10 to 60 μm across and consist of individual particles with diameters of approximately 0.1 to 10 μm (e.g., Figure 5A, C, G, I). Note that all SEM images displayed in Figures 5 and 7 were taken in BSE mode and that the EDX spectra were gathered from the full image in all cases. Most EDX spectra revealed that in addition to Pb, other elements, including Mg, Al, Si, K, Ca, Ti, and Fe, were present in the particles (e.g., Figure 5B, D, H, J), suggesting that the Pb-rich particles are mingled with various silicates and oxides. The phases previously identified with

XRD (Table 1), which included mainly quartz, dolomite, and feldspars, are consistent with this interpretation. SEM is a surface-sensitive technique (Kuisma-Kursula, 2000; Mosbah et al., 1995), and significant scatter of X-rays occurred during the investigation of our samples, because the sample surface is not flat, the particle size ranges widely, and the grains show non-uniform rounding and variable arrangements.

Dietrich et al. (2019, Figure 7) observed Pb-rich particles in street sediment, which were similar to those found in the Fishtown samples, including larger particles that are tens of micrometers in diameter composed of multiple smaller Pb-rich particles (Figure 5G). They further documented subhedral to euhedral particles of Pb that have diameters of 3 to 5 μm, analogous to those presented in Figure 5A and C. A small Pb-rich particle was observed in Figure 5K; the prominent Si peak (Figure 5L) associated with the image is inferred to be scatter from the adjacent lower-right grain, interpreted to be quartz. Other images (e.g., Figure 5I) demonstrate particles rich in Pb and, based on broad textural similarities to those described by Beard and Iske (1995), may show legacy Pb-house paint. Other particles contained Pb and Cr and were interpreted as degraded yellow traffic paint as they had textures consistent with those observed in past investigations (e.g., Figure 5E) (O'Shea et al., 2021; White et al., 2014). These textures are characterized by evenly distributed, submicrometer-sized subhedral to euhedral crystals of $PbCrO_4$ in an organic-rich matrix. Determining the nature and source of particles is crucial because those factors determine how or if particles are bioavailable/bioaccessible (e.g., Kelepertzis et al., 2021). Lead in house paint has been found to be 4–100% leachable in simulated gut fluid, whereas Pb in yellow traffic paint may be 1% leachable in simulated gut fluid (Le Bot et el., 2011; O'Shea et al., 2021).

Figure 5A, C, and I were taken from soil samples, whereas Figure 5E, G, and K were dust samples. Similar Pb-rich particles were found in both media. However, both the largest (Figure 5G) and smallest (Figure 5K) Pb-rich particles were found in road dust. Based on the similarity of Pb-rich particles overall, there is likely significant interaction and transport of particles between road dust and soils.

Brightfield TEM images, EDX spectra, and SAED images were collected in an attempt to identify some of the Pb-rich phases, which we inferred to be present based on SEM data. Only images for FS at Site 1 were displayed due to its richness in Pb (4,148 ppm) and because of instrument time constraints. Figure 6A–C shows data for a complex mineral aggregate containing O, P, K, Pb, and Zn, but dominated by Ca, Al, and Si. The SAED pattern (Figure 6C) shows weak and streaked diffraction spots, which are interpreted as resulting from multiple crystals giving rise to a ring diffraction pattern. The primary ring spacing is interpreted as the $d_{(104)}$ = 3.03 Å reflections of calcite, with weak and less developed reflections of $d_{(110)}$ = 2.49 Å, $d_{(113)}$ = 2.29 Å, $d_{(113)}$ = 1.88 Å. These reflections are consistent with ICDD 5–586 as well as Sitepu (2009). A few weak reflections are also interpreted to be arising from dolomite with $d_{(104)}$ = 2.88 Å; this reflection is consistent with ICDD 11–78. The EDX spectrum has significant Ca and O, and appreciable Mg (not marked on figure due to size constraints), which is consistent with calcite being a major component of the aggregate and dolomite being a lesser component. Indeed, both calcite and dolomite were identified in this sample with XRD (Table 1) and could stem from road material

(asphalt), sidewalk (concrete), and/or concrete construction materials (see also Gillott, 1978; El. Machi et al., 2021; O'Shea et al., 2020; Sommer et al., 2018). Aluminum, Si, P, Fe, and Ti are interpreted to be in poorly crystalline or amorphous phases in the aggregate. A distinct Pb-bearing phase was not identified. Similarly, Zn peaks were observed but no Zn-bearing phase was found. Both Zn and Pb are interpreted to be adsorbed onto carbonates and poorly crystalline clay phases.

Figure 6D–F displays an aggregate of Pb-rich particles, which also contain O, Si, Ca, and Fe. The SAED pattern presented (Figure 6F) is from the center cluster of crystals, i.e., from multiple crystals, and therefore mimics a powder pattern enabling identification of the dominant material. Numerous d-spacings observed in the diffraction rings indicate that the predominant phase is hydrocerussite ($Pb_3(CO_3)_2(OH)_2$). Specifically, these measured d-spacings are 4.47 Å, 2.63 Å, 2.24 Å, 2.02 Å, 1.88 Å, 1.64 Å, 1.49 Å, 1.35 Å, 1.30 Å, and 1.21 Å, and they are consistent with ICDD 13–131, and with Cowley (1956) and Martinetto et al. (2002). The comparatively high level of Pb in the EDX spectrum reinforces this identification. Hydrocerussite has historically been used as a pigment in white Pb paints (e.g., Beauchem et al., 2011; Van Alphen, 1998). Furthermore, the particles in Figure 5I were interpreted to be Pb paint. The presence of hydrocerussite supports the hypothesis that legacy paint plays a major role in soil-Pb contamination. Quantitative contents of both C and O cannot be obtained in Figure 6D owing to the lacey carbon grid used, and because Si, Fe, and Ca are likely bonded to O as silicates which are interpreted to be from the lower-contrast detrital particles in the aggregate (Figure 6E).

Figure 6G–I highlights a particle that was dominated by Ti and O, but also contained Pb and much lesser amounts of Al, Si, and Fe. The SAED pattern presented in Figure 6I is a square net with minor streaking and is interpreted to be an (hk0) net of rutile. The reflections observed include: $d_{(110)}$ = 3.24 Å, $d_{(210)}$ = 2.05 Å, $d_{(220)}$ = 1.62 Å, and $d_{(310)}$ = 1.45 Å, and are consistent with diffraction of rutile according to Swope et al. (1995). The dominant Ti lines (K_α = 4.509 keV and K_β = 4.934 keV) and the O line (K = 0.525) strongly support this interpretation. Therefore, this particle is likely rutile with minor amounts of Pb adhered or adsorbed to the surface. No distinct diffraction of other phases could be identified. This suggests that the detected Pb, Al, Si and Fe are contained in amorphous or poorly crystalline phases adhered to the surface of the crystal, as can be observed on the edges of the crystal displayed in the brightfield TEM image (Figure 6H). Rutile is a common pigment in paints, such as white paints and yellow traffic paint (e.g., O'Shea et al., 2021; White et al., 2014).

In addition to the Pb-rich particles, other phases were frequently observed during our SEM investigations (Figure 7). Figure 7A and 7C both display low-magnification BSE images of soil particles. Image 7A contains Mg, Al, Si, Pb, K, Ca, Ti, and Fe (spectrum shown in 7B); there is Al, Si, Pb, K, Ca, and Fe in image 7C (spectrum shown in 7D). Due to the generic textures of the majority of particles in both images, it is difficult to interpret the identity of individual particles. However, the EDX spectra from both images are consistent with minerals previously identified using XRD (Table 1), including quartz, feldspars, dolomite, and halloysite. Images 7A and C suggest that Pb occurs as diffuse particles throughout the samples at a scale not resolvable here but consistent with many particles observed in Figure 6. Image 7E displays particles with Fe, Al, Si, Ti, and Mn EDX peaks (Figure 7F).

The particles in the center of the image may be Fe-Ti oxides and Fe-oxides/oxyhydroxides and were interpreted as detrital grains and natural in origin as they had features similar to those of detrital oxides (e.g., Oglesbee et al., 2020). The Si signature could represent surrounding quartz, whereas the origin of Al and Mn was unclear. Figure 7G shows particles with Fe, Mg, Al, Si, S, Cl, K, Ca, Ti, Mn, and Cu EDX peaks (Figure 7H). The particles in the image are mainly Fe-oxide with minor amounts of Cu (Figure 7G–H). We propose that Cu is adsorbed onto these Fe-oxide particles (see also Langmuir, 1997; Martínez and McBride, 2001; Peacock and Sherman, 2004; Rose et al., 1993), because there is no clear phase contrast that would point to the presence of individual particles of Cu metal or other Cu phases. The Si present in Figure 7H was mainly interpreted as scatter from surrounding quartz, whereas the Ca and Mg could be related to nearby dolomite. Some of the Al and Si could be from clay minerals. The Cl and S could be from tire particles (e.g., Gieré et al., 2004). The origin of the remaining elements was uncertain and is interpreted to be from surrounding particles in the sample. Figure 7I and 7K both display high-contrast hackly fractured Fe-rich particles; the corresponding spectra also display significant Si, Ca, Al, and Mg peaks. The particles were interpreted as steel fragments similar to those documented in Dietrich et al. (2018), as they have high contrast, euhedral textures mixed with curvilinear edges and surfaces. The observed steel fragments contained approximately 1.31–2.48 at.% Mn, determined using data from the raw spectrum (not shown), and are consistent with the common ASTM A36 steel (e.g., Bhola et al. 2011) or similar steels. The Si present in both cases is interpreted as scatter from surrounding quartz and silicate minerals, whereas the Ca and Mg peaks are interpreted as scatter from nearby carbonate (calcite, dolomite). Similar to other samples studied with SEM above, owing to the sample surface not being flat, the wide range in particle size, the non-uniform rounding of grains, and the variable arrangement of grains, significant scatter of X-rays occurs.

Figure 7A, C, and E images were taken from soils, whereas Figure 7G, I, and K show road dust samples. Overall, Fe-oxides were demonstrated to occur in both media, and neighboring quartz, feldspars, and dolomite were potentially present in both road dust and soils. However, steel flakes were observed in only road dust. Some images were taken from collocated soil (e.g., Figure 7E), and dust (e.g., Figure 7G) samples. These images both demonstrate Fe-oxides but only the dust sample contained Cu. Due to the similarities observed, both media have similar sources and/or there is mixing of road dust and soil.

Implications

We describe a novel environmental media assessment, the first of its kind in Philadelphia. In Fishtown BD and FD, we identified element sources and mineral phases similar to those observed in a recent citywide study of bulk road dust (O'Shea et al., 2020).

The use of LOI, ICP-OES, laser diffraction, and XRD allowed us to constrain the potential sources and form of pollutants observed, with a focus on Pb. Combining these methods with SEM and TEM embodies a significant step forward in research on roadside pollution. This paper represents considerable progress in environmental assessments, not only because of the applied combination of diverse methods, but also because we investigated samples

of two collocated media and two different size fractions, thus yielding considerably deeper insights into the relationships between sources and sinks than most previous studies.

Summary and conclusions

The multi-pronged analytical approach utilized in this study created a data set that allows for comparison of road dust and soil in a polluted urban environment. By assessing both a bulk and a finer (<125 μm) size fraction from the same samples, this study will help in bridging the gap between previous bulk studies and health-relevant assessments.

The major findings of this study were: 1) Soil samples in Fishtown were heavily polluted with Pb, with higher concentrations in the finer fraction than in the bulk. The mean concentrations of Pb in both fine (687 ppm) and bulk (595 ppm) soils exceeded the 400 ppm EPA threshold, and they are high when compared internationally. 2) The soil samples collected closest to former Pb smelters were not those with the highest Pb contents. While further work must be performed, the lack of a clear relationship between former smelter locations and Pb-soil concentrations suggests that legacy paint and/or leaded-gasoline products are the main sources of the Pb present. 3) SEM investigations demonstrated that many of the Pb particles were micrometer- to submicrometer-sized; due to this small size and their abundance, the Pb particles could pose a health risk. 4) For most chemical elements investigated here, there were statistically significant differences in their concentration based on size fraction and medium using two-way analysis of variance tests. 5) Similar sources of contamination and mineralogical components were found in both road dust and soil, implying communication between the two media. Compared to most past work, the methods utilized broadened the scope of analysis, created a highly detailed dataset, improved the assessment of sources of pollution, and provided deep insights into the communication between road dust and road-side soils in a post-industrial environment at two size fractions. Going forward, we recommend focusing on finer, more health-relevant size fractions, utilizing a standard size fraction and a similar multi-analytical approach, and using both road dust and soil for more holistic assessments of contamination in urban environments.

Supplementary Material

Refer to Web version on PubMed Central for supplementary material.

Acknowledgements:

We thank the Benjamin Franklin Fellowship and the Greg and Susan Walker Foundation for support from the University of Pennsylvania. This work was further supported by the U.S. National Institute of Environmental Health Sciences (NIEHS) grant P30-ES013508, awarded to the University of Pennsylvania. The findings are not the official opinions of NIEHS or NIH. We thank the two anonymous reviewers and the editor for their assistance with improving the quality of the manuscript.

Funding:

This work was partially supported by grant P30-ES013508 awarded by the National Institute of Environmental Health Sciences (NIEHS). The findings are not the official opinions of NIEHS or NIH. This work was also supported by the University of Pennsylvania (Benjamin Franklin Fellowship) and the Greg and Susan Walker Foundation. The funding bodies did not play a role in the study itself.

Availability of data and material:

Data generated and/or analyzed during this study are included in this published article (supplemental). For more information, please contact the corresponding author.

References

Acosta JA, Gabarrón M, Faz A, Martínez-Martínez S, Zornoza R, Arocena JM, 2015. Influence of population density on the concentration and speciation of metals in the soil and street dust from urban areas. Chemosphere134, 328–337. 10.1016/j.chemosphere.2015.04.038 [PubMed: 25966939]

Adimalla N, Chen J, Qian H, 2020. Ecotoxicology and Environmental Safety Spatial characteristics of heavy metal contamination and potential human health risk assessment of urban soils : A case study from an urban region of. Ecotoxicol. Environ. Saf194, 110406. 10.1016/j.ecoenv.2020.110406 [PubMed: 32151868]

Agency for Toxic Substances and Disease Registry, 2019. Toxicological Profile for Lead. Draft for public commentAtlanta, GA.

Akbar KF, Hale WHG, Headley AD, Athar M (2006). Heavy metal contamination of roadside soils of Northern England. Soil Water Res 1(4):158–163. 10.17221/6517-SWR

Alves DD, Riegel RP, Klauck CR, Ceratti AM, Hansen J, Cansi LM, Pozza SA, de Quevedo DM, Osório DMM, 2020. Source apportionment of metallic elements in urban atmospheric particulate matter and assessment of its water-soluble fraction toxicity. Environ. Sci. Pollut. Res12202–12214. 10.1007/s11356-020-07791-8

Amato F, Pandolfi M, Escrig A, Querol X, Alastuey A, Pey J, Perez N, Hopke PK, 2009. Quantifying road dust resuspension in urban environment by Multilinear Engine: A comparison with PMF2. Atmos. Environ43, 2770–2780. 10.1016/j.atmosenv.2009.02.039

Apeagyei E, Bank MS, Spengler JD, 2011. Distribution of heavy metals in road dust along an urban-rural gradient in Massachusetts. Atmos. Environ45, 2310–2323. 10.1016/j.atmosenv.2010.11.015

Ball DF, 1964. Loss on Ignition As an Estimate of Organic Matter and Organic Carbon in Non Calcareous Soils. J. Soil Sci15, 84–92. 10.1111/j.1365-2389.1964.tb00247.x

Barnes M, McLeod C, Faraci O, Chappell C, Krekeler MPS (2020) Characterizing the geogenic background of the Midwest: A detailed mineralogical and geochemical investigation of a glacial till in southwestern Ohio. Environmental Earth Sciences 79:159.

Bavec Š, Biester H, Gosar M, 2014. Urban sediment contamination in a former Hg mining district, Idrija, Slovenia. Environ. Geochem. Health36, 427–439. 10.1007/s10653-013-9571-6 [PubMed: 24114255]

Beard MIske SDA (1995). Lead in Paint, Soil and Dust: Health Risks, Exposure Studies, Control Measures, Measurement Methods, and Quality Assurance. ASTM Publication Code Number (PCN) 04-012260-17 https://www.unicoil.com.sa/wp-content/uploads/2017/04/astm-lead.pdf

Beauchemin S, MacLean LCW, Rasmussen PE, 2011. Lead speciation in indoor dust: a case study to assess paint contribution in a Canadian urban house. Environ. Geochem. Health, 33, 343–352. [PubMed: 21465232]

Bernardino CAR, Mahler CF, Santelli RE, Freire AS, Braz BF, Novo LAB, 2019. Metal accumulation in roadside soils of Rio de Janeiro, Brazil: impact of traffic volume, road age, and urbanization level. Environ. Monit. Assess191. 10.1007/s10661-019-7265-y

Bhola SM, Bhola R, Jain L, Mishra B, Olson DL, 2011. Corrosion Behavior of Mild Carbon Steel in Ethanolic Solution. JMEPEG20, 409–416.

Biasioli M, Barberis R, Ajmone-Marsan F, 2006. The influence of a large city on some soil properties and metals content. Sci. Total Environ356, 154–164. 10.1016/j.scitotenv.2005.04.033 [PubMed: 15941578]

Calabrese EJ, Stanek EJ, James RC, and Roberts SM (1997). Soil ingestion: A concern for acute toxicity in children. Environ. Health Perspect 105, 1354–1358. [PubMed: 9405323]

Cal-Prieto MJ, Carlosena A, Andrade JM, Martínez ML, Muniategui S, López-Mahía P, Prada D (2001) Antimony as a tracer ofthe anthropogenic influence on soils and estuarine sediments. Water Air Soil Pollut 129 (1–4):333–348. 10.1023/A:1010360518054

Christoforidis A, Stamatis N, 2009. Heavy metal contamination in street dust and roadside soil along the major national road in Kavala's region, Greece. Geoderma151, 257–263. 10.1016/j.geoderma.2009.04.016

Chen X, Xia X, Zhao Y, Zhang P (2010) Heavy metal concentrations in roadside soils and correlation with urban traffic in Beijing, China. J Hazard Mater 181(1–3):640–646. 10.1016/j.jhazmat.2010.05.060 [PubMed: 20541319]

Councell TB, Duckenfield KU, Landa E, Callender E2004. Tire-wear particles as a source of zinc to the environment. Environ. Sci. Technol38, 4206–4214. [PubMed: 15352462]

Council on Environmental Health, 2016. Prevention of Childhood Lead Toxicity. Pediatrics138. 10.1542/peds.2016-1493

Cowley JM (1956) Electron-diffraction study of the structure of basic lead carbonate $2PbCO_3{\cdot}Pb(OH)_2$, Acta Crystallographica 9: 391–396

Cymes BA, Almquist C, Krekeler MPS (2020) Europium-doped cryptomelane: Multi-pathway synthesis, characterization, and evaluation for the gas phase catalytic oxidation of ethanol. Applied Catalysis A, General 589: 117310.

Dannis ML1974. Rubber dust from the normal wear of tire. Rubber Chemistry and Technology47(4) 1011–1037.

Dao L, Morrison L, Zhang H, Zhang C (2014) Influences of traffic on Pb, Cu and Zn concentrations in roadside soils of an urban park in Dublin, Ireland. Environ Geochem Health 36(3):333–343. 10.1007/s10653-013-9553-8 [PubMed: 23828236]

Davis S, Mirick DK. 2006. Soil ingestion in children and adults in the same family. J Expo Sci Environ Epidemiol16(1):63–75. 10.1038/sj.jea.7500438. [PubMed: 16047041]

Delaware Valley Regional Planning Commision (DVRPC). "Traffic Count Viewer". Scale Not Given. "DVRPC Traffic Count Viewer"102, 2016. https://www.opendataphilly.org/dataset/traffic-count-viewer

De Silva S, Ball AS, Huynh T, Reichman SM, 2016. Metal accumulation in roadside soil in Melbourne, Australia: Effect of road age, traffic density and vehicular speed. Environ. Pollut208, 102–109. 10.1016/j.envpol.2015.09.032 [PubMed: 26603093]

Dietrich M, Huling J, Krekeler MPS, 2018. Metal pollution investigation of Goldman Park, Middletown Ohio: Evidence for steel and coal pollution in a high child use setting. Sci. Total Environ618, 1350–1362. 10.1016/j.scitotenv.2017.09.246 [PubMed: 29111254]

Dietrich M, Wolfe A, Burke M, Krekeler MPS, 2019. The first pollution investigation of road sediment in Gary, Indiana: Anthropogenic metals and possible health implications for a socioeconomically disadvantaged area. Environ. Int128, 175–192. [PubMed: 31059913]

Duong TTT, Lee BK, 2011. Determining contamination level of heavy metals in road dust from busy traffic areas with different characteristics. J. Environ. Manage92, 554–562. 10.1016/j.jenvman.2010.09.010 [PubMed: 20937547]

Elom NI, Entwistle J, Dean JR (2014). Human health risk from Pb in urban street dust in northern UK cities. Environ. Chem. Lett 12, 209–218.

El. Machi A, Mabroum S, Taha Y, Tagnit-Hamou A, Bezazzoua M, Hakkou R2021. Valorization of phosphate mine waste rocks as aggregates for concrete. Materialstoday: Proeddings, 37(3), 3840–3846.

Esri. (2017) "Worldmap" [basemap]. 1:1,000. "World Street Map"910. http://www.arcgis.com/home/item.html?id=3b93337983e9436f8db950e38a8629af

Faiz Y, Tufail M, Tayyeb Javed M, Chaudhry M, 2009. Road dust pollution of Cd, Cu, Ni, Pb and Zn along Islamabad Expressway, Pakistan. Microchem. J92, 186–192. 10.1016/j.microc.2009.03.009

Ferreira-Baptista L, De Miguel E, 2005. Geochemistry and risk assessment of street dust in Luanda, Angola: A tropical urban environment. Atmos. Environ39, 4501–4512. 10.1016/j.atmosenv.2005.03.026

Filippelli GM, Laidlaw M, Latimer J, Raftis R (2005). Urban lead poisoning and medical geology: an unfinished story. GSA Today 15, 4–11.

Filippelli GM, Risch M, Laidlaw MAS, Nichols DE, & Crewe J (2015). Geochemical legacies and the future health of cities: A tale of two neurotoxins in urban soils. Elementa, 3, 000059.

Filippelli G, Anenberg S, Taylor M, Geen A, Khreis H, 2020. New Approaches to Identifying and Reducing the Global Burden of Disease From Pollution. GeoHealth4, 1–25. 10.1029/2018gh000167

Flett L, Krekeler MPS, Burke M, 2016. Investigations of road sediment in an industrial corridor near low-income housing in Hamilton, Ohio. Environ. Earth Sci75. 10.1007/s12665-016-5945-2

Frank JJ, Poulakos AG, Tornero-Velez R, Xue J, 2019. Systematic review and meta-analyses of lead (Pb) concentrations in environmental media (soil, dust, water, food, and air) reported in the United States from 1996 to 2016. Sci. Total Environ694, 133489. 10.1016/j.scitotenv.2019.07.295 [PubMed: 31756826]

Gaberšek M, Gosar M, 2018. Geochemistry of urban soil in the industrial town of Maribor, Slovenia. J. Geochemical Explor187, 141–154. 10.1016/j.gexplo.2017.06.001

Gaberšek M, Grcman H, Gosar M, 2020. Mineral composition, pedological characteristics and fractionation of selected chemical elements in soil of maribor. Geologija62/2, 177–191.

Gaberšek M, Gosar M, 2021. Towards a holistic approach to the geochemistry of solid inorganic particles in the urban environmentt. Science of the Total Environment763, 144214.

Gieré R, LaFree ST, Carleton LE, Tishmack JK, 2004. Environmental impact of energy recovery from waste tyres. In: Giere RStille P (eds): Energy, Waste, and the Environment: a Geochemical Perspective. Geological Society, London, Special Publications 236, 475–498.

Gieré R, Smith W, Bandemehr A, Pepino R, Howarth M, Wyman M (2020). The need to eliminate lead paint globally. United Nations Environment Programme Foresight Brief 1–6

Gillott JE1978. Effect of deicing agents and sulphate solutions on concrete aggregate. Quarterly Journal of Engineering Geology and Hydrogeology11, 177–192. 10.1144/GSL.QJEG.1978.011.02.06

Gunawardana C, Goonetilleke A, Egodawatta P, Dawes L, Kokot S (2012). Source characterization of road dust based on chemical and minerlaogical composition. Chemosphere 87, 163–170. [PubMed: 22209254]

Han X, Lu X, Qinggeletu WY (2017). Health risks and contamination levels of heavy metals in dusts from parks and squares of an industrial city in semi-arid area of China. Int. J. Environ. Res. Public Health 14, 886.

Harrison RM, Jones AM, Gietl J, Yin J, Green DC, 2012. Estimation of the Contributions of Brake Dust, Tire Wear, and Resuspension to Nonexhaust Traffic Particles Derived from Atmospheric Measurements. Environ. Sci. Technol46, 6523–6529. 10.1021/es300894r [PubMed: 22642836]

Herngren L, Goonetilleke A, Ayoko GA. (2006) Analysis of heavy metals in road-deposited sediments. Anal Chim Acta571:270–278 [PubMed: 17723448]

Hiller E, Pilková Z, Filová L, Jurkovič Ľ, Mihaljevič M, Lacina P, 2020. Concentrations of selected trace elements in surface soils near crossroads in the city of Bratislava (the Slovak Republic). Environ. Sci. Pollut. Res10.1007/s11356-020-10822-z

Jiao W, Chen W, Chang AC, Page A2012. Environmental risks of trace elements associated with long-term phosphate fertilzers applications: a review. Environmental Pollution168, 44–53. [PubMed: 22591788]

Kelepertzis E, Argyraki A, Chrastný V, Botsou F, Skordas K, Komárek M, Fouskas A, 2020. Metal(loid) and isotopic tracing of Pb in soils, road and house dusts from the industrial area of Volos (central Greece). Sci. Total Environ725, 138300. 10.1016/j.scitotenv.2020.138300 [PubMed: 32302831]

Kelepertzis E, Chrastný V, Botsou F, Sigala E, Kypritidou Z, Komárek M, Skordas K, Argyraki A (2021). Tracing the sources of bioaccessible metal(loid)s in urban environments: A multidisciplinary approach. Sci. Total Environ 771, 144827. [PubMed: 33529817]

Ko S, Schaefer PD, Vicario CM, Binns HJ, 2007. Relationships of video assessments of touching and mouthing behaviors during outdoor play in urban residential yards to parental perceptions of child behaviors and blood lead levels. J. Expo. Sci. Epidemiol17, 47–57.

Komárek M, Ettler V, Száková J, Šebek O, Tlustoš P, 2009. Bioavailability of lead and cadmium in soils artificially contaminated with smelter fly ash. Bull. Environ. Contam. Toxicol83, 286–290. 10.1007/s00128-009-9742-4 [PubMed: 19424651]

Kong S, Lu B, Bai Z, Zhao X, Chen L, Han B, Li Z, Ji Y, Xu Y, Liu Y, Jiang H, 2011. Potential threat of heavy metals in re-suspended dusts on building surfaces in oilfield city. Atmos. Environ45, 4192–4204. 10.1016/j.atmosenv.2011.05.011

Kuisma-Kursula P, 2000. Accuracy, precision and detection limits of SEM-WDS, SEM-EDS and PIXE in the multi-element analysis of medieval glass. X Ray Spectrom29, 111–118.

Laidlaw MAS, Filippelli GM, 2008. Resuspension of urban soils as a persistent source of lead poisoning in children: A review and new directions. Appl. Geochemistry23, 2021–2039. 10.1016/j.apgeochem.2008.05.009

Laidlaw MAS, Taylor MP, 2011. Potential for childhood lead poisoning in the inner cities of Australia due to exposure to lead in soil dust. Environ. Pollut159, 1–9. 10.1016/j.envpol.2010.08.020 [PubMed: 20880621]

Laidlaw MAS, Zahran S, Mielke HW, Taylor MP, Filippelli GM, 2012. Re-suspension of lead contaminated urban soil as a dominant source of atmospheric lead in Birmingham, Chicago, Detroit and Pittsburgh, USA. Atmos. Environ49, 302–310. 10.1016/j.atmosenv.2011.11.030

Laidlaw MAS, Filippelli GM, Brown S, Paz-Ferreiro J, Reichman S, Netherway P, Truskewycz A, Ball A, & Mielke H (2017). Case studies and evidence-based approaches to addressing urban soil lead contamination. Applied Geochemistry, 83, 14–30.

Langmuir D (1997) Aqueous Environmental Geochemistry Upper Saddle River, N.J. Prentice Hall.

Lanphear BP, Hornung R, Khoury J, Yolton K, Baghurst P, Bellinger DC, Canfield RL, Dietrich KN, Bornschein R, Greene T, Rothenberg SJ, 2005. Low-level environmental lead exposure and children's intellectual function: an international pooled analysis. Environ. Health Perspect1, 894–899.

Lanphear BP, Matte TD, Rogers J, Clickner RP, Dietz B, Bornschein RLet al. (1998). The contribution of lead-contaminated house dust and residential soil to children's blood lead levels. A pooled analysis of 12 epidemiologic studies. Environmental Research 79, 51–68. 10.1006/enrs.1998.3859 [PubMed: 9756680]

Lanzerstorfer C, 2020. Toward more intercomparable road dust studies. Crit. Rev. Environ. Sci. Technol0, 1–30. 10.1080/10643389.2020.1737472

Lanzerstorfer C, 2018. Heavy metals in the finest size fractions of road-deposited sediments. Environ. Pollut239, 522–531. 10.1016/j.envpol.2018.04.063 [PubMed: 29684879]

Latimer JC, Van Halen D, Speer J, Krull S, Weaver P, Pettit J, Foxx H, 2016. Soil lead testing at a high spatial resolution in an urban community garden: a case study in relic lead in Terre Haute, Indiana. J. Environ. Health79, 28–35.

Le Bot B, Arcelin C, Briand E, Glorennec P, 2011. Sequential digestion for measuring leachable and total lead in the same sample of dust or paint chips by ICP-MS. J. Environ. Sci. Heal. - Part A Toxic/Hazardous Subst. Environ. Eng46, 63–69. 10.1080/10934529.2011.526902

Legalley E, Krekeler MPS, 2013. A mineralogical and geochemical investigation of street sediment near a coal-fired power plant in Hamilton, Ohio: An example of complex pollution and cause for community health concerns. Environ. Pollut176, 26–35. 10.1016/j.envpol.2012.12.012 [PubMed: 23395990]

Liang SY, Cui JL, Bi XY, Luo XS, Li XD, 2019. Deciphering source contributions of trace metal contamination in urban soil, road dust, and foliar dust of Guangzhou, southern China. Sci. Total Environ695, 133596. 10.1016/j.scitotenv.2019.133596 [PubMed: 31421330]

Lim SS, et al., 2012. A comparative risk assessment of burden of disease and injury attributable to 67 risk factors and risk factor clusters in 21 regions, 1990–2010: A systematic analysis for the Global Burden of Disease Study 2010. Lancet380, 2224–2260. 10.1016/S0140-6736(12)61766-8 [PubMed: 23245609]

Liu E, Yan T, Birch G, Zhu Y, 2014. Pollution and health risk of potentially toxic metals in urban road dust in Nanjing, a mega-city of China. Sci. Total Environ476–477, 522–531. 10.1016/j.scitotenv.2014.01.055

Lu X, Wang L, Li LY, Lei K, Huang L, Kang D, 2010. Multivariate statistical analysis of heavy metals in street dust of Baoji, NW China. J. Hazard. Mater173, 744–749. 10.1016/j.jhazmat.2009.09.001 [PubMed: 19811870]

Lusby G, Hall C, Reiners J, 2015. Lead Contamination of Surface Soils in Philadelphia from Lead Smelters and Urbanization. Environ. Justice8, 6–14. 10.1089/env.2014.0008

MacKinnon G, MacKenzie AB, Cook GT, Pulford ID, Duncan HJ, Scott EM, 2011. Spatial and temporal variations in Pb concentrations and isotopic composition in road dust, farmland soil and vegetation in proximity to roads since cessation of use of leaded petrol in the UK. Sci. Total Environ409, 5010–5019. 10.1016/j.scitotenv.2011.08.010 [PubMed: 21907389]

Malkoc S, Yazıcı B, Koparal S (2010). Assessment of the levels of heavy metal pollution in roadside soils of Eskisehir, Turkey. Environ Toxicol Chem 29(12):2720–2725. 10.1002/etc.35 [PubMed: 20836060]

Martinetto P, Anne M, Dooryhee E, Walter P, Tsoucaris G (2002) Synthetic hydrocerussite, $2PbCO_3{\cdot}Pb(OH)_2$ by X-ray powder diffraction. Acta Crystallographica C58, 82–84.

Martinez CE, McBride MB, 2001. Cd, Cu, Pb, and Zn Coprecipitates in Fe Oxide Formed at different pH: aging effects on metal solubility and extractability by citrate. Environmental Chemistry20(1), 122–126.

Mielke HW, Gonzales CR, Powell ET, Laidlaw MA, Berry KJ, Mielke PW, Egendorf SP, 2019. The concurrent decline of soil lead and children's blood lead in New Orleans. Proc. Natl. Acad. Sci. Unit. States Am116, 22058–22064.

Mosbah M, Clocchiatti R, Metrich N, Piccot D, Rio S, Titira J (1995) The characterization of glass inclusions through nuclear microprobe. Nuclear Instruments and Methods in Physics Research B 104, 271–275.

Novotny V, & Chesters G (1981). Handbook of nonpoint pollution sources and management (pp. 441–445). Van Nostrand Reinhold: New York.

NOAA (National Oceanic and Atmospheric Administration). Station Name: PA PHILADELPHIA INTL APNational Oceanic and Atmospheric Administration. RetrievedAugust 16th, 2019.

Oglesbee T, McLeod C, Chappell C, Vest J, Sturmer D, Krekeler MPS (2020) A Mineralogical and Geochemical Investigation of Modern Aeolian Sands near Tonopah, Nevada: Sources and Environmental Implications. Catena 194: 104640

Okorie A, Entwistle J, Dean JR (2012). Estimation of daily intake of potetentially toxic elements from urban street dust and the role of oral bioaccessibility testing Chemosphere 86, 460–467. [PubMed: 22024094]

O'Shea MJ, Vann DR, Hwang WT, Gieré R, 2020. A mineralogical and chemical investigation of road dust in Philadelphia, PA, USA. Environ. Sci. Pollut. Res27, 14883–14902. 10.1007/s11356-019-06746-y

O'Shea MJ, Vigliaturo R, Choi JK, McKeon TP, Krekeler MPS, Gieré R, 2021. Alteration of yellow traffic paint in simulated environmental and biological fluids. Sci. Total Environ750. 10.1016/j.scitotenv.2020.141202

Ordóñez A, Loredo J, De Miguel E, Charlesworth S, 2003. Distribution of heavy metals in the street dusts and soils of an industrial city in Northern Spain. Arch. Environ. Contam. Toxicol44, 160–170. 10.1007/s00244-002-2005-6 [PubMed: 12520388]

Padoan E, Romè C, Ajmone-Marsan F, 2017. Bioaccessibility and size distribution of metals in road dust and roadside soils along a peri-urban transect. Sci. Total Environ601–602, 89–98. 10.1016/j.scitotenv.2017.05.180

Pant P, Harrison RM, 2013. Estimation of the contribution of road traffic emissions to particulate matter concentrations from field measurements: A review. Atmos. Environ77, 78–97. 10.1016/j.atmosenv.2013.04.028 Review

Paul KC, **Silverstein J, Krekeler MPS (2017) New insights into rare earth element particulate generated by cigarette lighters: an electron microscopy and materials science investigation of a poorly understood indoor air pollutant and constraints for urban geochemistry. Environmental Earth Sciences 76: 369

Peacock CL, Sherman DM, 2004. Copper (II) sorption onto goethite, hematite and lepidocrocite: A surfface complexation model based on ab initio molecular geometries and EXAFS spectroscopy. Geochimica et Cosmochimica Acta86(12), 2623–2637.

Pennsylvania Department of Environmental Protection. (2021a). Land Recycling Program, Site Completed, Southeast regionhttp://cedatareporting.pa.gov/Reportserver/Pages/ReportViewer.aspx?/Public/DEP/LRP/SSRS/LandRecycling_Sites_Complete.Accessed, November 20, 2020.

Pennsylvania Department of Environmental Protection. (2021b). Land Recycling Program, Site in Progress, Southeast regionhttp://cedatareporting.pa.gov/Reportserver/Pages/ReportViewer.aspx?/Public/DEP/LRP/SSRS/LandRecycling_Sites_Progress Accessed, November 20, 2020.

Pichery C, Bellanger M, Zmirou-Navier D, Glorennec P, Hartemann P and Grandjean P (2011). Childhood lead exposure in France: benefit estimation and partial cost-benefit analysis of lead hazard control. Environmental Health 10(1), 44. 10.1186/1476-069X-10-44 [PubMed: 21599937]

Qiao X, Schmidt AH, Tang Y, Xu Y, Zhang C (2014) Demonstrating urban pollution using toxic metals of road dust and roadside soil in Chengdu, South Western China. Stochastic Environmental Research Risk Assessment 28, 911–919.

Rose AW, Bianchi G, 1993. Adsorption of Cu, Pb, Zn, Co, Ni, and Ag on goethite and hematite; a control on metal mobilization from red beds into stratiform copper deposits. Economic Geology88(5), 1226–1236.

Ruby MV, Lowney YW, 2012. Selective soil particle adherence to hands: Implications for understanding oral exposure to soil contaminants. Environ. Sci. Technol46, 12759–12771. 10.1021/es302473q [PubMed: 23148503]

Ruderman W, Laker B, & Purcell D (2017a). "In booming Philadelphia neighborhoods, lead-poisoned soil is resurfacing." The Philadelphia Inquirer, Philadelphia Media Network, https://www.inquirer.com/news/inq/philadelphia-lead-soil-fishtown-construction-dust-20170618.html. Accessed June 2017.

Ruderman W, Laker B, & Purcell D (2017b). "Toxic City: State confirms extreme lead levels in Kensington soil." The Philadelphia Inquirer, Philadelphia Media Network, https://www.inquirer.com/philly/news/toxic-city-state-confirms-extreme-lead-levels-in-kensington-soil-20181018.html Accessed December 2017.

Rudnick RL, Gao S (2003) Composition of the continental crust. Treatise Geochem 3:1–64. 10.1016/B0-08-043751-6/03016-4

Scranton PFigured Tapestry: Production, markets, and power in Philadelphia textiles, 1885–1941, Cambrige University Press: New York, 1989. Print.

Sommer F, Dietze V, Baum A, Sauer J, Gilge S, Maschowski CGiere R (2018). Tire abrasion as a major source of microplastics in the environment. Aerosol and Air Quality Research 18, 2014–2028.

Shi G, Chen Z, Bi C, Wang L, Teng J, Li Y, Xu S, 2011. A comparative study of health risk of potentially toxic metals in urban and suburban road dust in the most populated city of China. Atmos. Environ45, 764–771. 10.1016/j.atmosenv.2010.08.039

Shotyk W, Weiss D, Heisterkamp M, Cheburkin AK, Appleby PG, and Adams FC2002. New peat bog record of atmospheric lead pollution in Switzerland: Pb concentrations, enrichment factors, isotopic composition, organolead species. Environmental Science &Technology, 36 (18), 3893–3900. DOI: 10.1021/es010196i

Siciliano S, James K, Zhang G, Schafer A, Peak D, 2009. Adhesion and Enrichment of Metals on Human Hands from Contaminated Soil at an Arctic Urban Brownfield. Environ. Sci. Technol43, 6385–6390. [PubMed: 19746741]

Sitepu H (2009) Texture and structural refinement using neutron diffraction data form molybdite (MoO_3) and calcite (CaO_3) powders and a Ni-rich $Ni_{50.7}Ti_{49.30}$ alloy. Powder Diffraction 24: 315–326.

Smith E, Weber J, Naidu R, McLaren RG, Juhasz AL, 2011. Assessment of lead bioaccessibility in peri-urban contaminated soils. J. Hazard. Mater186, 300–305. 10.1016/j.jhazmat.2010.10.111 [PubMed: 21115224]

Stanek EJ, Calabrese EJ, Barnes R, et al.1997. Soil ingestion in adults--results of a second pilot study. Ecotoxicol Environ Saf36(3):249–257. 10.1006/eesa.1996.1510. [PubMed: 9143453]

Stanek EJ, Calabrese EJ, Xu B2012. Meta-analysis of mass-balance studies of soil ingestion in children. Risk Anal32(3):433–447. 10.1111/j.1539-6924.2011.01673.x. [PubMed: 21883335]

Swope RJ, Smyth JR, Larson AC (1995) H in rutile-type compounds: I. Single-crystal neutron and X-ray diffraction study of H in rutile. American Mineralogist 80: 448–453.

Teran K, Žibret G, Fanetti M, 2020. Impact of urbanization and steel mill emissions on elemental composition of street dust and corresponding particle characterization. J. Hazard. Mater384, 120963. 10.1016/j.jhazmat.2019.120963 [PubMed: 31628063]

Thorpe A, Harrison RM, 2008. Sources and properties of non-exhaust particulate matter from road traffic: A review. Sci. Total Environ400, 270–282. 10.1016/j.scitotenv.2008.06.007 [PubMed: 18635248]

Tong S, von Schirnding YE, Prapamontol T, 2000. Environmental lead exposure. Bull. World Health Organ23, 112–118. 10.1016/S0165-6147(00)01972-6

Turner A, Kearl ER, Solman KR, 2016. Science of the Total Environment Lead and other toxic metals in playground paints from South West England. Sci. Total Environ544, 460–466. 10.1016/j.scitotenv.2015.11.078 [PubMed: 26657391]

Turner A, Sogo YSK, 2012. Chemosphere Concentrations and bioaccessibilities of metals in exterior urban paints. Chemosphere86, 614–618. 10.1016/j.chemosphere.2011.10.045 [PubMed: 22113057]

Turner A, Solman KR, 2016. Science of the Total Environment Lead in exterior paints from the urban and suburban environs of. Sci. Total Environ547, 132–136. 10.1016/j.scitotenv.2015.12.125 [PubMed: 26780138]

United Nations (2014), Department of Economic and Social Affairs, Population Division. World urbanization prospects: the 2014 revision, highlights (ST/ESA/SER.A/352)

US Environmental Protection Agency. (1996). Method-3050B. Acid digestion of sediments, sludges, and soilsWashington, DC.

US Environmental Protection Agency. (2001). 40 CFR part 745. Lead; identification of dangerous levels of lead: final rule. Fed Regist66(4):1206–1240

Van Alphen M (1998). Paint film components. National environmental health forum monographs, General series no. 2, Glenelg Press, Australia.

Varrica D, Dongarrà G, Sabatino G, Monna F, 2003. Inorganic geochemistry of roadway dust from the metropolitan area of Palermo, Italy. Environ. Geol44, 222–230. 10.1007/s00254-002-0748-z

Wei B, Yang L, 2010. A review of heavy metal contaminations in urban soils, urban road dusts and agricultural soils from China. Microchem. J94, 99–107. 10.1016/j.microc.2009.09.014

Wei X, Gao B, Wang P, Zhou H, Lu J, 2014. Pollution characteristics and health risk assessment of heavy metals in street dusts from different functional areas in Beijing, China. Ecotoxicol. Environ. Saf112, 186–192. 10.1016/j.ecoenv.2014.11.005 [PubMed: 25463870]

Weiss D, Shotyk W, Appleby PG, Kramers JD, Cheburkin AK, 1999. Atmospheric Pb deposition since the industrial revolution recorded by five Swiss peat profiles: enrichment factors, fluxes, isotopic composition, and sources. Environmental Science &Technology, 33 (9), 1340–1352, DOI: 10.1021/es980882q

Weiss J, 1949. Wissahickon Schist At Philadelphia, Pennsylvania. Bull. Geol. Soc. Am60, 1689–1726.

White K, Detherage T, Verellen M, Tully J, Krekeler MPS, 2014. An investigation of lead chromate (crocoite-PbCrO4) and other inorganic pigments in aged traffic paint samples from Hamilton, Ohio: Implications for lead in the environment. Environ. Earth Sci71, 3517–3528. 10.1007/s12665-013-2741-0

Wik A, Dave G2009. Occurrence and effects of tire wear particles in the environment - A critical review and an intial risk assessment. Environmental Pollution157(1), 1–11. 10.1016/j.envpol.2008.09.028 [PubMed: 18990476]

Zannoni D, Valotto G, Visin F, Rampazzo G, 2016. Sources and distribution of tracer elements in road dust: The Venice mainland case of study. J. Geochemical Explor166, 64–72. 10.1016/j.gexplo.2016.04.007

Zgłobicki W, Telecka M, Skupiński S, 2019. Assessment of short-term changes in street dust pollution with heavy metals in Lublin (E Poland)—levels, sources and risks. Environ. Sci. Pollut. Res35049–35060. 10.1007/s11356-019-06496-x

Zhao H, Li X, Wang X, Tian D, 2010. Grain size distribution of road-deposited sediment and its contribution to heavy metal pollution in urban runoff in Beijing, China. J. Hazard. Mater183, 203–210. 10.1016/j.jhazmat.2010.07.012 [PubMed: 20674162]

Zhao L, Hu G, Yan Yu, Yu R, Cui J, Wang X, Yan Yan, 2019. Source apportionment of heavy metals in urban road dust in a continental city of eastern China: Using Pb and Sr isotopes combined with multivariate statistical analysis. Atmos. Environ201, 201–211. 10.1016/j.atmosenv.2018.12.050

Žibret G, Van Tonder D, Žibret L, 2013. Metal content in street dust as a reflection of atmospheric dust emissions from coal power plants, metal smelters, and traffic. Environ. Sci. Pollut. Res20, 4455–4468. 10.1007/s11356-012-1398-7

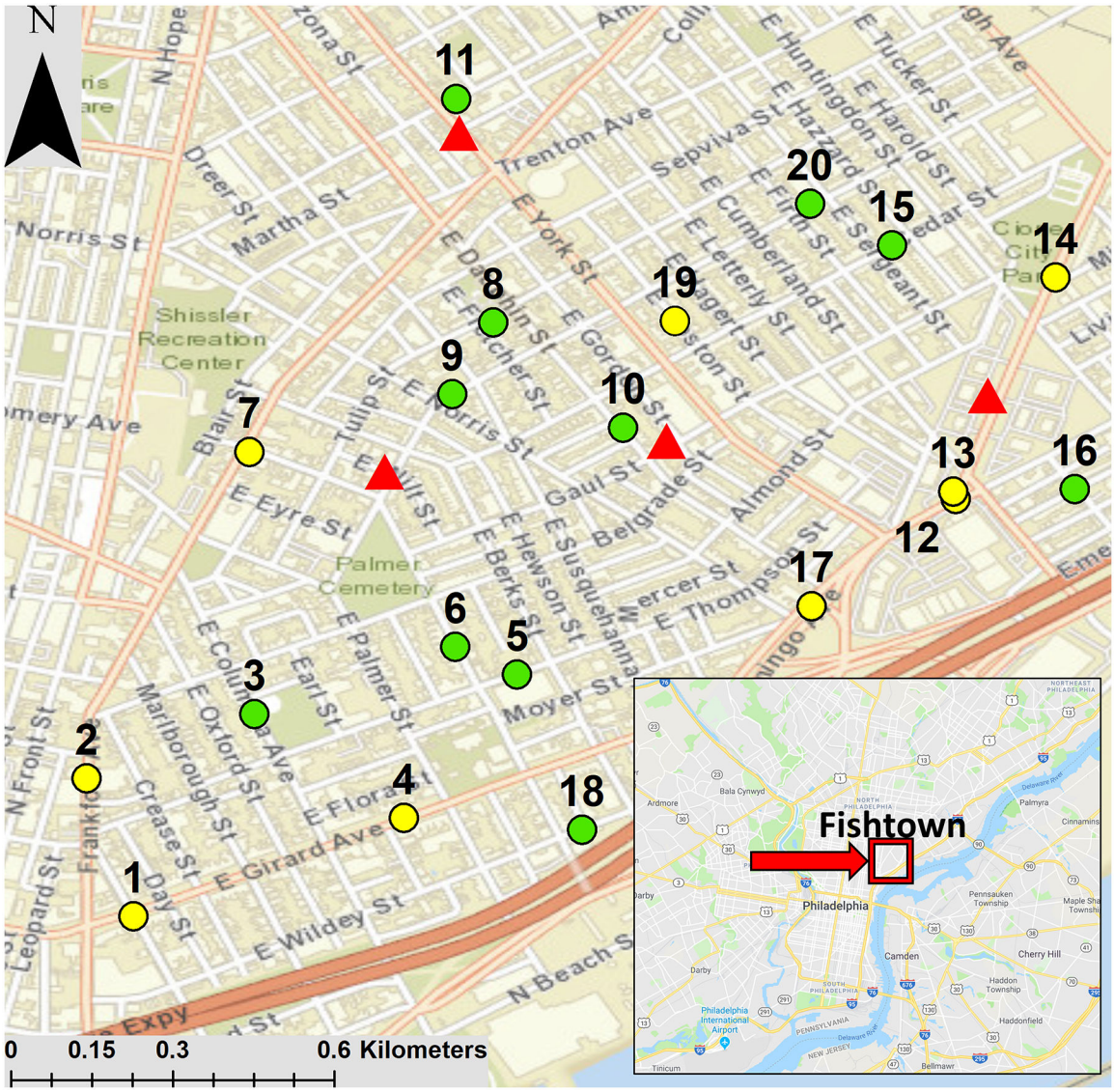

Figure 1:

Locations of road dust and soil sampling sites in Fishtown, Philadelphia. Lower traffic (defined as <6,000 annual average daily traffic (AADT)) sites are green and higher traffic (defined as ≥6,000 AADT) sites are yellow. Data from the Delaware Valley Regional Planning Commission (DVRPC, 2016). Locations of former smelters are shown with red triangles. The map was generated in ArcGIS (Esri, 2017) and the inset image from Google maps

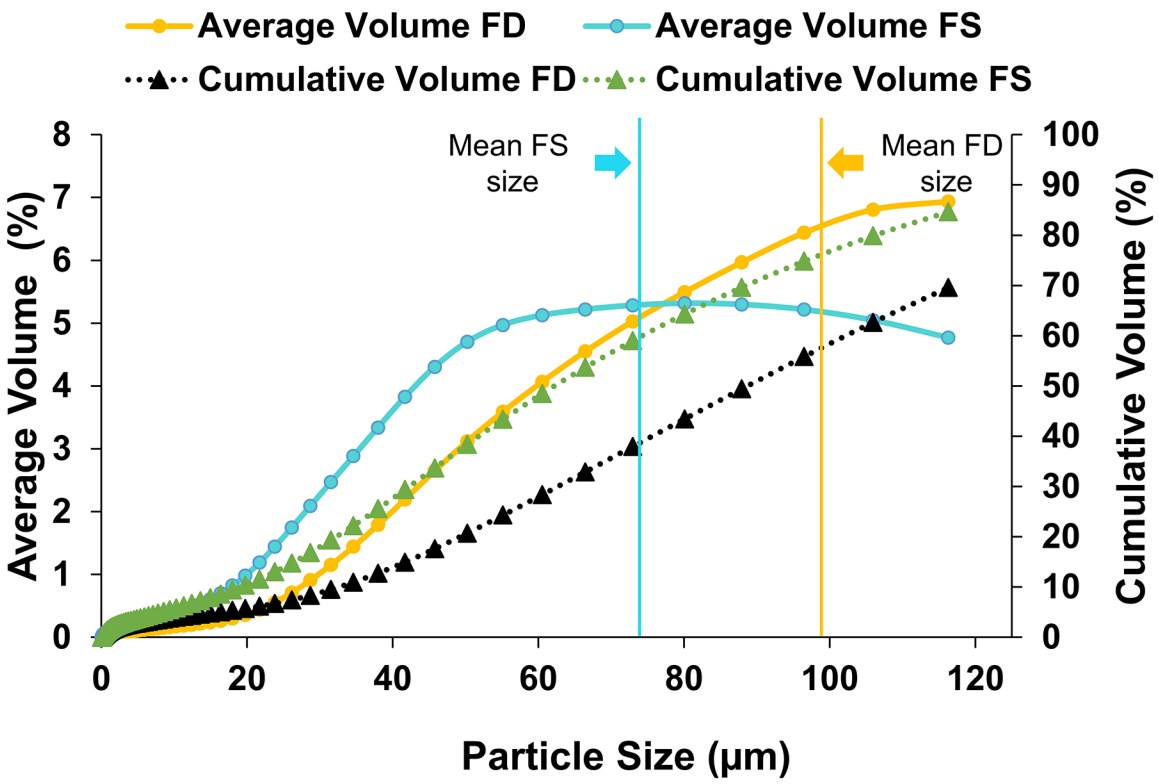

Figure 2:

Average particle size distribution of the finer fractions of road dust and soil (fine dust [FD], $n = 20$; fine soil [FS], $n = 20$) after ashing. Standard volume per size fraction is on the y-axis, whereas cumulative volume is on the y-axis to the right

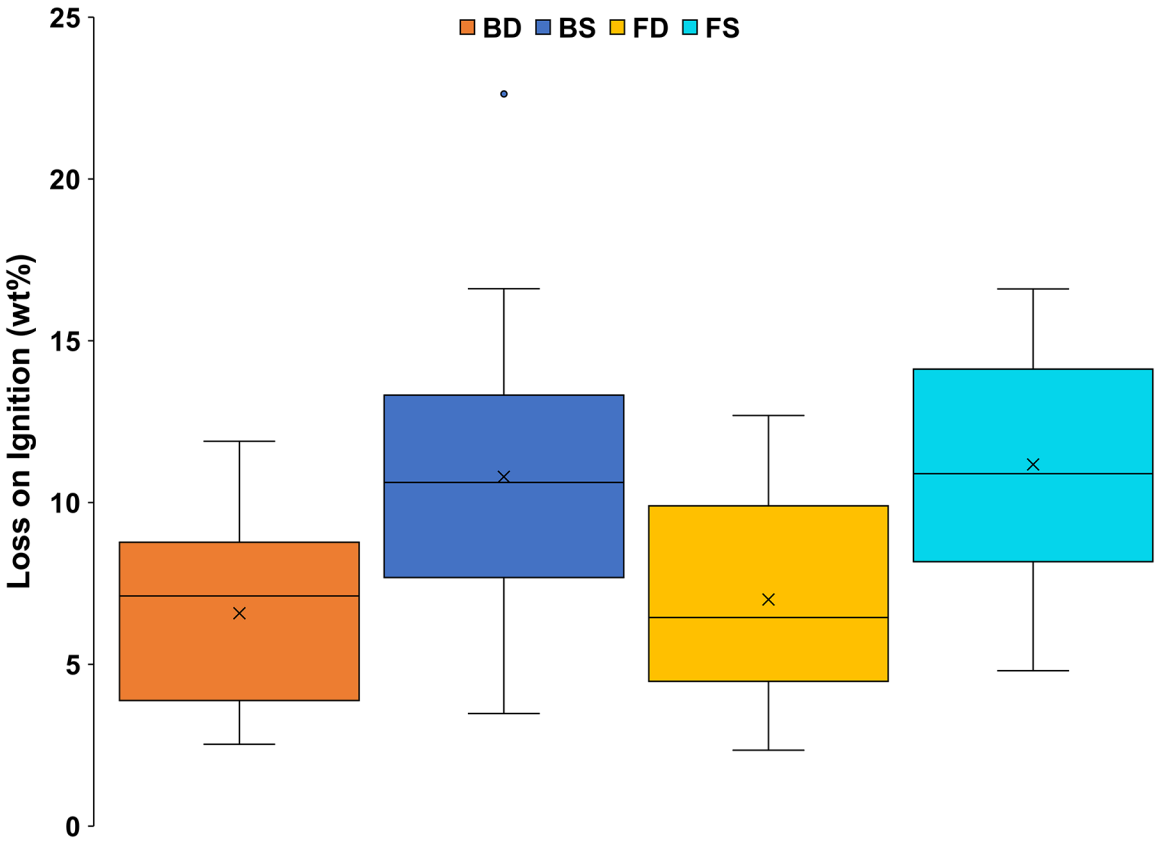

Figure 3:
Box and whisker plot of LOI results (in wt%) for bulk dust (BD), bulk soil (BS), fine dust (FD), and fine soil (FS). The x represents mean value, whereas the horizontal line is median value. All points outside of the boxes (IQR) and whiskers (min. and max. values—excluding outliers) are outliers (1.5× below the 1st quartile or 1.5× above the 3rd quartile)

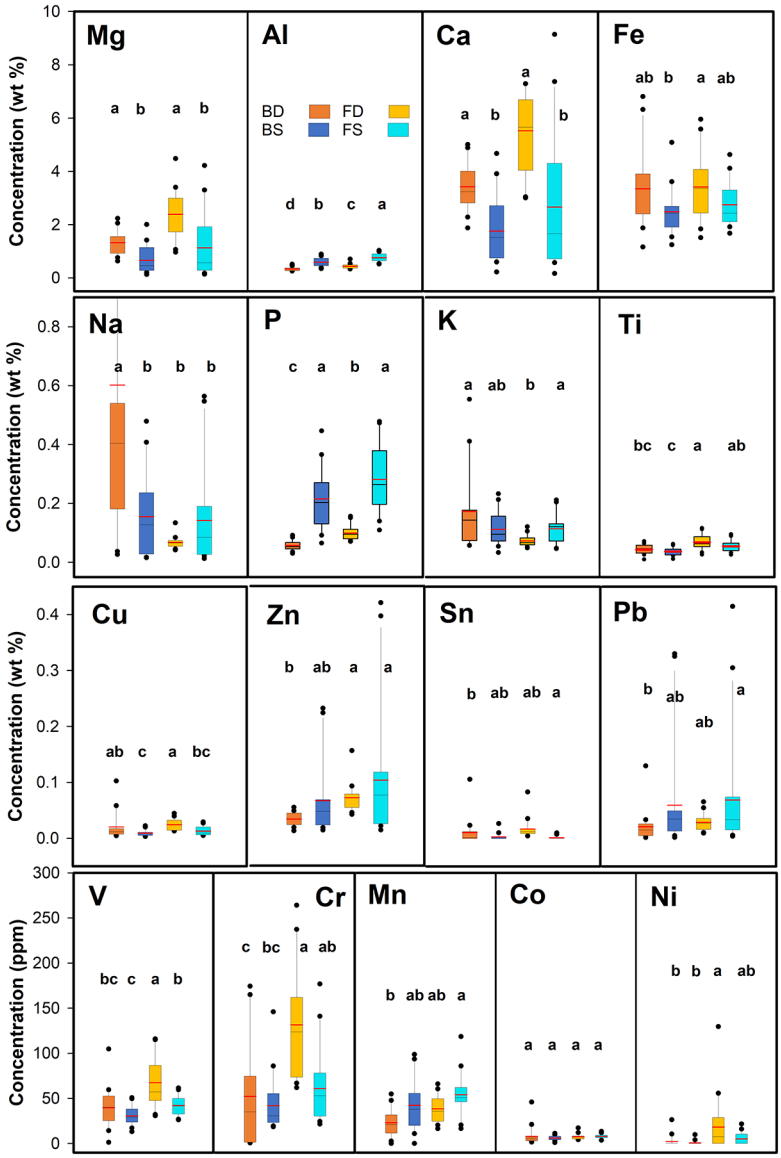

Figure 4:

Acid-extractable elemental concentrations for bulk dust (BD), bulk soil (BS), fine dust (FD), and fine soil (FS). Boxes represent 25th-75th percentiles; horizontal lines are median (black) and mean (red). Vertical line is 10th to 90th percentile. Dots are outliers. Outliers of 3.67 wt% and 1.73 wt% Na (BD) and 10.71 wt% Ca (FD) were omitted. The letters (a, b, c, d) represent the results of Tukey's honestly significant difference (HSD) post-hoc tests which were performed following the two-way ANOVA tests listed in Table 2. Boxes shown with different letters are statistically significantly different ($p<0.05$). If a group is not significantly different from two other groups, but the two other groups are different from each other, two letters will be assigned to the first group, to indicate that it is not different from the other two

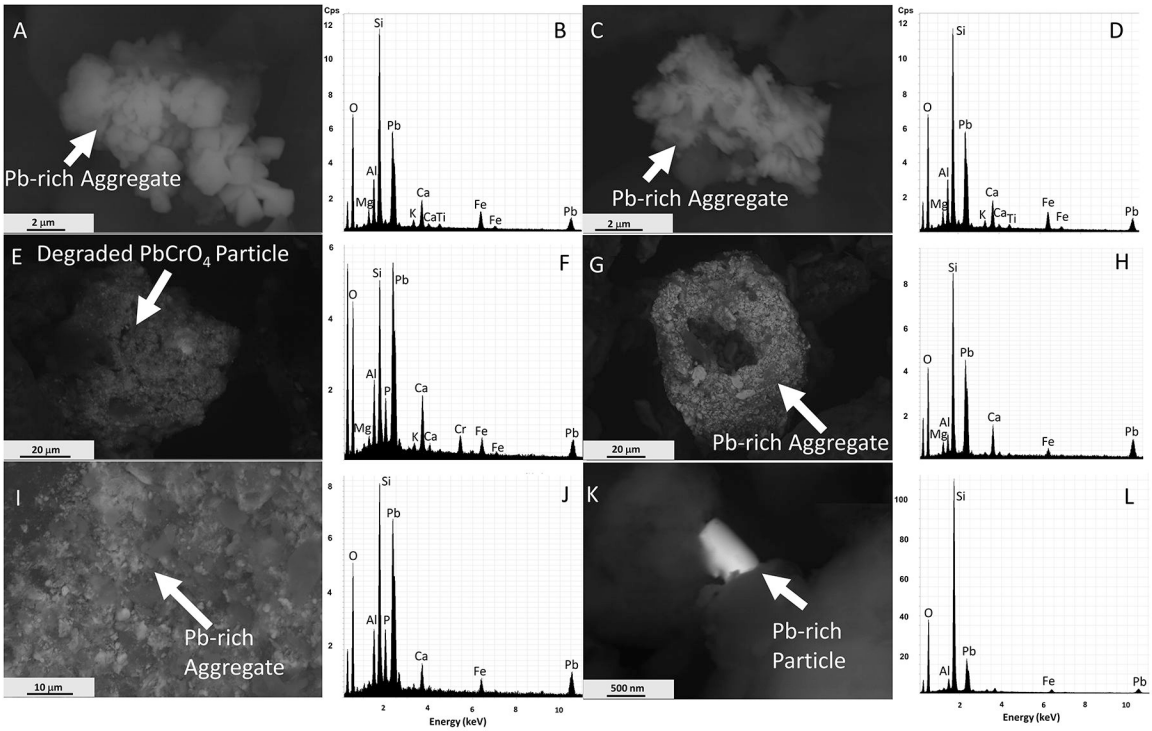

Figure 5:

SEM images and corresponding EDX spectra of Pb particles found in road dust and soil. Most Pb particles were on the micrometer scale. (A) BSE image and (B) EDX spectrum of a Pb-rich particle from FS at Site 1, demonstrating a commonly observed aggregate texture with numerous 0.1 to 3 µm diameter particles. The Mg, Al, Si, K, Ca, Ti and Fe peaks are from mineralogical substrate material; (C) BSE image and (D) EDX spectrum of a Pb-rich particle showing an aggregate texture commonly observed in FS at Site 1. Elements other than Pb are interpreted to be derived from the mineralogical substrate; (E) BSE image and (F) EDX spectrum of a degraded $PbCrO_4$ particle from FD at Site 10, possibly from yellow traffic paint; (G) BSE image and (H) EDX spectrum of a Pb-rich aggregate from FD at Site 5, largely composed of numerous 0.1 to 3 µm diameter particles with some larger 10 µm diameter particles present; (I) BSE image and (J) EDX spectrum of Pb-containing particles approximately 0.1 to 3 µm in diameter from BS at Site 1, possibly Pb paint; (K) BSE image and (L) EDX spectrum of a nanoscale Pb-rich particle from BD at Site 5. Note: the first major peak not labeled in any of the spectra is carbon. The images were cropped at 12 keV, omitting minor Pb peaks at 12.3 keV and 14.35 keV

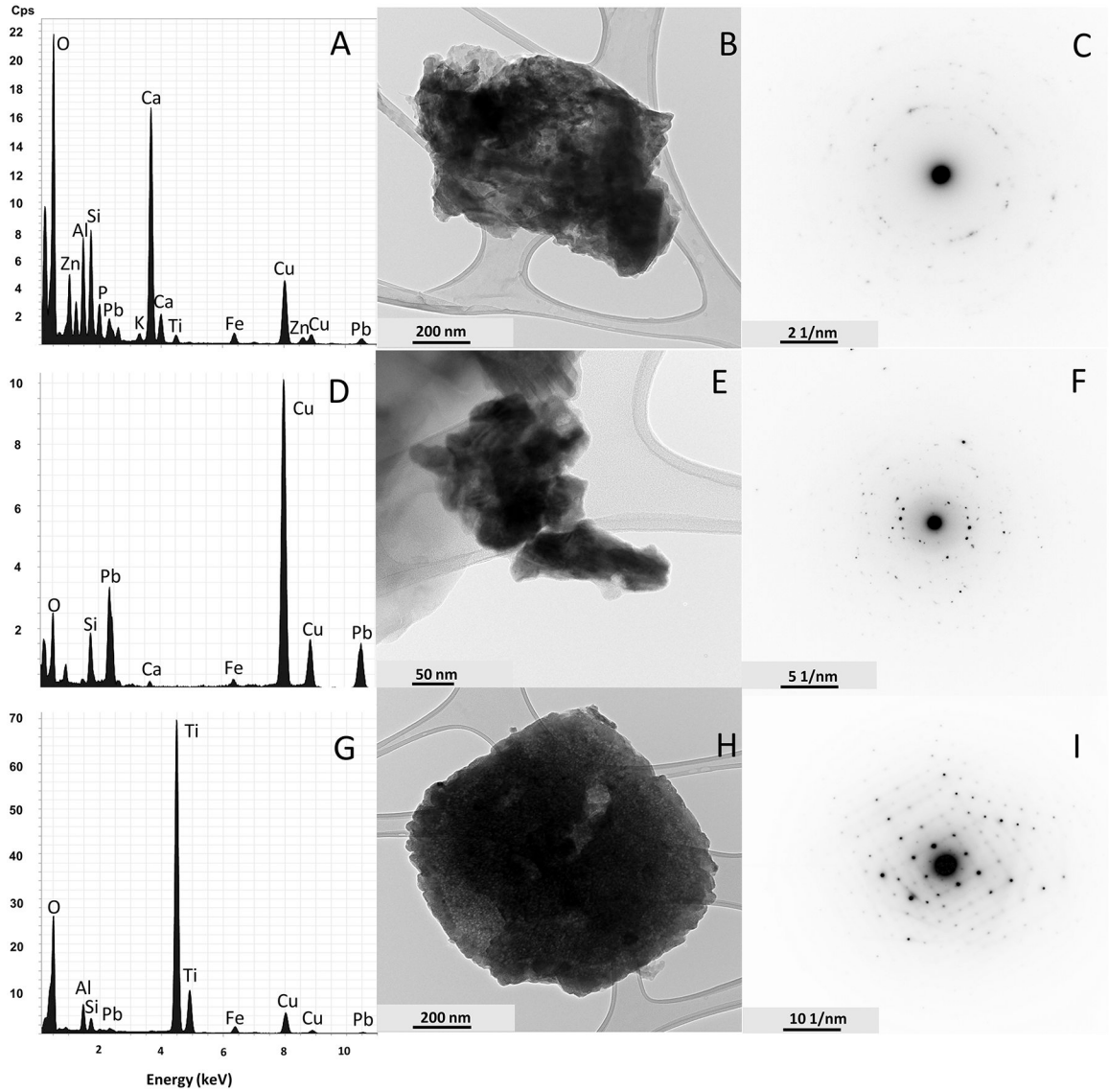

Figure 6:

EDX spectra, Brightfield TEM images, and selected-area electron diffraction (SAED) patterns of particles observed. All images are from FS at Site 1. (A) EDX spectrum, (B) TEM image, and (C) SAED pattern of a calcite- and dolomite-rich particle with Pb; (D) EDX spectrum, (E) TEM image, and (F) SAED pattern of a hydrocerussite Pb-rich particle; (G) EDX spectrum, (H) TEM image, and (I) SAED pattern of a rutile particle with Pb. Note: the first major peak not labeled in any of the spectra is carbon. The images were cropped at 12 keV, omitting minor Pb peaks at 12.3 keV and 14.35 keV. Peaks at 8 keV and 8.45 keV are representative of the Cu grid rather than the sample

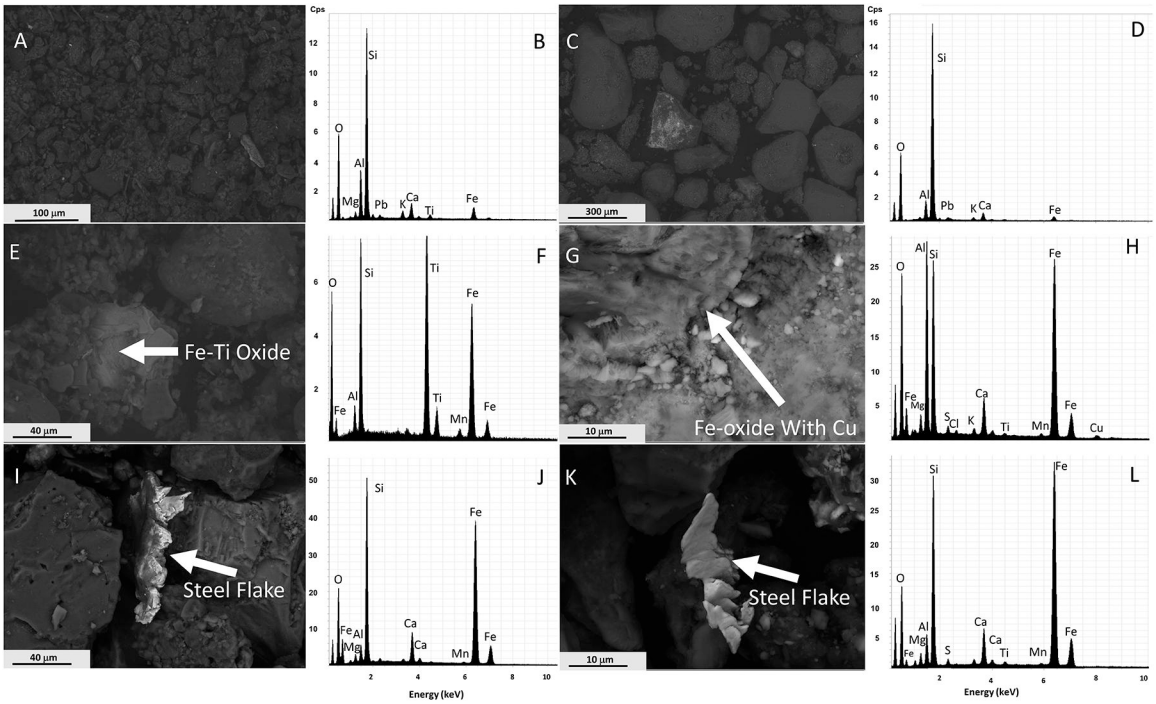

Figure 7:

SEM images and corresponding EDX spectra of common particles found in road dust and soil. (A) BSE image and (B) EDX spectrum of FS material from Site 1; (C) BSE image and (D) EDX spectrum of BS material from Site 1; (E) BSE image and (F) EDX spectrum of an Fe-Ti oxide particle present in BS at Site 1; (G) BSE image and (H) EDX spectrum of an Fe-oxide particle with Cu present in FD from Site 1; (I) BSE image and (J) EDX spectrum of a steel flake in FD from Site 4; (K) BSE image and (L) EDX spectrum of a different steel particle in FD from Site 4. Note: the first major peak not labeled in any of the spectra is carbon.

Table 1:

Sample site number, brief site descriptions, and mineral phases identified (wt%) at each site for bulk dust (BD), bulk soil (BS), fine dust (FD), and fine soil (FS).

Site	Description	Quartz				Dolomite/Calcite				Feldspar[2]				Other			
		BD	BS	FD	FS	BD	BS	FD	FS	BD	BS	FD	FS	BD	BS	FD	FS
1	Commercial	53	?	60	76	9	?	10[1]	8[1]	38	?	30	16		?(H)		
2	Commercial	65	74	47	89	9		9		26	6	44	11		20(M)		
3	Near Playground	41	70	50	6	16	17[1]	18	41[1]	41*	13	32	53	2(M)			
4	Commercial	48	81	39	8	20	9	6[1]	53[1]	32	10	55	39				
5	Near School	53	90	59	91	37		9		10	10	32	9				
6	South of Palmer Cemetery	49	92	51	91	28		26		13	8	23	9	9(M)			
7	Near Recreation Center	74	95	76	83	12	5	7	5	14		17	12				
8	Konrad Sq. Park – Church	61	92	68	40	21[1]		14		18	4	18	4		4(M)		56(M)
9	Smelter[3]/Near Palmer Cemetery	62	96	81	91	17[1]		11[1]		21	3	8	9		1(C)		
10	Near Gaul St. Smelter[3]	61	86	76	37	12[1]		10		27	14	14	7				56(M)
11	Near E. York St. Smelter[3]	77	92	63	79	19	4	25[1]	10	4	4	12	11				
12	Aramingo Ave. Lower Traffic	86	98	49	82	6	2	24	4	8		27	14				
13	Aramingo Ave. Higher Traffic	85	?	61	73	8	?	8	9	7	?	31	18		?(H)		
14	Cione City Park	89	97	67	80	7	3	15	6	4		18	14				
15	Aramingo Square	90	89	94	97	10[1]	6	6	3						5(R)		
16	Neighborhood/ Commercial	66	89	57	69	17	1	16	3	13	10	27	9	4(M)			19(M)
17	Near Highway	60	85	19	37	22	8	46	7	18	7	35	2				54(M)
18	Near Chem. Corp.	90	60	94	69	10[1]	28[1]	6	6		12*		25*				
19	Neighborhood	83	75	72	32	12	10	9	12	5*		19*	7		15(M)		49(M)
20	Neighborhood	72	86	71	94	13[1]		7		15*	14	22*	6				

[1]Calcite present. Calcite was found in only 15 of 80 samples, with concentrations generally 3 wt% or less, except for sites 4 FS (12 wt%) and 11 FD (5 wt%). As calcite and dolomite are often found together and can be components of road aggregate, sidewalk (concrete), and/or concrete construction materials, these values were combined under one column labeled Dolomite/Calcite.

[2]Feldspar was identified as albite, except where marked by *, which means anorthite.

[3]Former smelter sites.

For other phases, C is chlorite; H is halloysite; M is mica; R is rutile; ? indicates that the quantities could not be determined.

Table 2-

Logscale two-way ANOVA results of elemental concentrations by size and media with P values listed. Interaction terms were calculated and listed. N.S. stands for not significant.

Element	Media (P Value)	Size (P Value)	Interaction Term (P Value)
Na	N.S.	<0.001	<0.005
Mg	<0.0001	<0.005	N.S.
Al	<0.0001	<0.0001	N.S.
P	<0.0001	<0.0001	N.S.
K	N.S.	<0.005	<0.002
Ca	<0.0001	<0.05	N.S.
Ti	<0.05	<0.0001	N.S.
Fe	<0.005	N.S.	N.S.
V	<0.001	<0.0001	N.S.
Cr	N.S.	<0.001	<0.003
Mn	<0.05	<0.005	N.S.
Co	N.S.	<0.05	N.S.
Ni	N.S.	<0.005	<0.002
Cu	<0.0001	<0.005	N.S.
Zn	N.S.	<0.001	N.S.
Sn	N.S.	<0.005	<0.002
Pb	<0.02	N.S.	N.S.

Table 3 -

Summary of results from factor analysis. Dominant elements in each factor, arranged in order of factor loading weight. Only factor loadings >0.40 were listed. Bold text denotes factor loading ≥ 0.90. Numerical percentage is cumulative variance. N/A denotes factors not present. (Additional details in Tables S5a, S5b, S7a, and S7b).

Medium	**Major Elements**							
	Factor 1	**%**	**Factor 2**	**%**	**Factor 3**	**%**	**Factor 4**	**%**
Bulk Dust	**Mg**, **Ca**, P	33	**Al**, Ti, Fe, P	65	**Na**, K	91	N/A	-
Bulk Soil	**Mg**, **Ca**, Al	33	**K**, Al, P, Na	58	**Ti**, Na, Al	77	Fe, Al, P	95
Fine Dust	**Mg**, **Ca**, K	33	**Fe**, **Na**, Ti	64	**P**, K, Al	93	N/A	-
Fine Soil	**Ca**, **Mg**, Na, Fe	42	K, Ti, Al	73	Fe, Al	88	N/A	-
	Minor Elements							
Bulk Dust	**Co**, V, Mn	34	**Cr**, Sn, Zn	56	Pb, Cu, Zn	76	Ni, Cu, Mn	94
Bulk Soil	**Mn**, V, Co	35	Pb, Cu	56	Cr, Cu, Ni	76	Sn, V	90
Fine Dust	**Ni**, **Cr**, Mn, Cu, Zn, Co	46	V, Co	72	Pb, Sn	88	N/A	-
Fine Soil	Cr, Cu, Ni, Zn, Sn	34	Pb, V, Cu	58	**Co**, Mn	80	N/A	-

Table 4 -

International comparison of selected element concentrations (in ppm) in bulk soil with those reported in previous urban soil studies. Median values are shown by normal font and mean by italic font.

City	Cu	Zn	Pb	Reference	Digestive Fluid Composition	Sieve Size (μm)
Philadelphia, PA	*92*	*663*	*595*	This study	$HCl+HNO_3$	<841
Beijing, China	*29.7*	*92.1*	*35.4*	Chen et al., 2010	HNO_3+HClO_4+HF	<150
Bratislava, Slovakia	*67.1*	*174*	*54.2*	Hiller et al., 2020	*	<2000
Dublin, Ireland	25.0	94.0	39.0	Dao et al., 2014	*	<2000
Eskisehir, Turkey	31.2	55.8	21.9	Malkoc et al., 2010	HNO_3	<50
Guangzhou, China	35.2	126	49.4	Liang et al., 2019	HNO_3+HClO_4	<2000
La Coruna, Spain	*60*	*206*	*309*	Cal-Prieto et al., 2001	Unspecified	<200
Maribor, Slovenia	40	131	44	Gaberšek and Gosar, 2018	$HCl+HNO_3$	<2000
Turin, Italy	100	242	133	Padoan et al., 2017	$HCl+HNO_3$	<150
Yorkshire, England	80.4	150.0	175.0	Akbar et al., 2006	$HCl+HNO_3$	<2000

*Samples were analyzed with portable X-Ray fluorescence (PXRF) spectrometers, which does not require a digestion. See original manuscripts for additional details.